

Fundamental constants from photon-photon scattering in three-beam collisions

Alexander J. MacLeod^{1,*} and Ben King²

¹*ELI Beamlines Facility, The Extreme Light Infrastructure ERIC,
Za Radnicí 835, 25241 Dolní Břežany, Czech Republic*

²*Centre for Mathematical Sciences, University of Plymouth, PL4 8AA, UK*

Direct measurement of the elastic scattering of real photons on an electromagnetic field would allow the fundamental low-energy constants of quantum electrodynamics (QED) to be experimentally determined. We show that scenarios involving the collision of three laser beams have several advantages over conventional two-beam scenarios. The kinematics of a three-beam collision allows for a higher signal-to-noise ratio in the detection region, without the need for polarimetry and separates out contributions from different orders of photon scattering. A planar configuration of colliding a photon beam from an x-ray free electron laser with two optical beams is studied in detail. We show that measurements of elastic photon scattering and vacuum birefringence are possible with currently available technology.

I. INTRODUCTION

Quantum electrodynamics (QED) predicts that the coupling between strong electromagnetic fields mediated by virtual particle/anti-particle pairs imbues the vacuum with nonlinear properties. This breaks the superposition principle of classical electrodynamics, allowing for the self interaction of electromagnetic fields. Microscopically, this self interaction corresponds to photon-photon scattering. Despite being predicted almost a century ago [1–6] a direct measurement of on-shell photon-photon scattering and the predicted birefringence of the quantum vacuum have yet to be made, although Delbrück scattering [7, 8] (the scattering of photons in a Coulomb field of a nucleus, i.e. involving off-shell photons) and more recently scattering of quasi-real photons in ultra-peripheral collisions of heavy ions in the ATLAS [9, 10] and CMS [11] experiments have been observed. It has also been reported [12] that the STAR [13] experiment measured an indirect signal of vacuum birefringence in the spectrum of electron-positron pairs created in ultra-peripheral heavy-ion collisions. The lack of verification of photon-photon scattering with real photons can be attributed to two obstacles: the small size of the photon-photon scattering cross section and the high background generated when colliding beams of photons. As laser technology continues to improve and provide photon sources with an ever-higher flux, experimental verification of real photon-photon scattering seems achievable. There have been numerous suggestions for how to increase the signal-to-noise ratio in discovery experiments employing intense laser pulses, such as ‘vacuum diffracting’ a probe beam with an intense pump beam [14–21], ‘vacuum reflection’ [22], frequency up/down-shifting [20, 23–25], suggestions to enhance the vacuum polarisation signal by using structured laser pulses [19, 25–27], and strategies to optimise the vacuum polarisation signal [28, 29]. Experimental verification of real photon-

photon scattering is particularly interesting as it provides the gateway to harnessing the nonlinear response of the vacuum for more exotic applications such as self-focussing [30], vacuum high harmonic generation [31, 32] and vacuum shock waves [33, 34] (for reviews on photon-photon scattering and strong-field QED see, e.g. [35–38]). Furthermore, with construction planned for lasers in the 10–100 PW range [39–43], real photon-photon scattering becomes more easily measurable as technology progresses (see also [44–49]).

In the current paper, we highlight the benefits of using a three-beam set-up to detect photon scattering and experimentally determine the fundamental low-energy constants of QED. The leading-order process is four-photon scattering and by colliding three beams the kinematics of the signal photons can be more directly specified. Early three-beam experiments [50] were performed that bounded the cross-section for the process, while investigations in the literature [23, 51–54] and a recent study on signal optimisation [28] have shown how a three-beam set-up can produce a change in: i) the polarisation, ii) the momentum, and iii) the energy of scattering photons, which can all be used to increase the signal-to-noise ratio. The results we present show that the fundamental low-energy constants of QED, which govern the magnitude of photon-photon scattering and associated phenomena such as vacuum birefringence, could be directly measured with today’s technology in a three-beam configuration which collides an x-ray beam with two optical laser pulses. This complements studies that have bounded combinations of these constants using results from laser-cavity experiments [55] and recent work suggesting colliding two beams to reach the sensitivity required to measure the values of these constants predicted by QED [56]. The most stringent bound on the fundamental low-energy constants has so far been made by the PVLAS laser-cavity experiment [57], which by searching for vacuum birefringence has placed a bound on the difference of the two lowest energy constants.

A key advantage of the three-beam set-up is that, by an appropriate choice of the collision geometry, signal photons can be scattered out of the probe beam such that in

* alexander.macleod@eli-beams.eu

the detector plane there is a spatial separation of signal and background. This allows for the photon count to be used as the signal, without requiring extra polarimetry (which, however, for x-ray photons is now sensitive to one in over ten billion [58]) or special modification of the probe beam [56]. If the probe is an x-ray free electron laser (XFEL), as we consider here, since no extra polarimetry is required there is no requirement on having an especially low bandwidth in the XFEL beam, which in turn allows one to use the self-amplified by spontaneous emission (SASE) [59, 60] mode with a higher photon flux to increase the signal. Should a measurement of vacuum birefringence be desired, this can also be facilitated with a three-beam set-up.

A further highlight of the three-beam configuration is that the kinematics also allow for spatially-separated signals of $2n$ -photon scattering. This should be compared to the two-beam configuration, which heavily suppresses scattering for $n > 2$. To investigate this point, the current work includes both 4-photon and 6-photon scattering processes. This allows us to go beyond previous studies and calculate the sensitivity required to access the fundamental low-energy constants of dimension-8 and dimension-10 operators.

We begin in Sec. II with some theory background, specify the collision geometry in Sec. III, detail the analytical results in Sec. IV, and numerical results in Sec. V. The paper concludes in Sec. VI. Extra technical detail on the beam profiles can be found in the Appendix, which features analysis of the infinite Rayleigh length approximation (IRLA) when an angular cut is applied to the scattered field.

II. THEORY BACKGROUND

The nonlinear interaction between photons mediated by virtual electron-positron pairs can be re-cast as an effective field theory with a Lagrangian expressed as a double sum of derivatives and powers of field strengths,

$$\mathcal{L}_{\text{eff}} = \sum_{\sigma, n} c_{\sigma, n}^{\text{eff}} \partial^{(\sigma)} \mathcal{O}^n, \quad (1)$$

where σ counts the number of derivatives and n the number of field strengths in the operator \mathcal{O} . The coefficients $c_{\sigma, n}^{\text{eff}}$ are *fundamental low-energy constants*. When the centre-of-momentum energy, ω_* , is much lower than the electron rest mass, m_e , and the field strength is much lower than the Sauter-Schwinger critical field¹, $E_{\text{cr}} = m_e^2/e \approx 1.3 \times 10^{16} \text{ Vcm}^{-1}$ (with m_e and $e > 0$ the mass and charge on a positron respectively), the physics can be described by the weak-field expansion of

the Heisenberg-Euler Lagrangian [3–5], $\mathcal{L}_{\text{eff}} \approx \mathcal{L}_{\text{HE}}$ with

$$\begin{aligned} \mathcal{L}_{\text{HE}} &= \frac{m_e^4}{\alpha} \sum_{n=2} \mathcal{L}_{2n}, \\ \mathcal{L}_4 &= \frac{\alpha}{360\pi^2} [c_{4,1} \mathcal{F}^2 + c_{4,2} \mathcal{G}^2], \\ \mathcal{L}_6 &= \frac{\alpha}{630\pi^2} [c_{6,1} \mathcal{F}^3 + c_{6,2} \mathcal{F} \mathcal{G}^2], \end{aligned} \quad (2)$$

Here, $\alpha = e^2/4\pi$ is the QED fine-structure constant, $c_{2n,j}$ are the fundamental low-energy constants, and throughout we normalise field strengths, e.g. in the Faraday tensor $F^{\mu\nu}$ and its dual $\tilde{F}^{\mu\nu}$, by the critical field E_{cr} . The (normalised) EM invariants are then $\mathcal{F} = -F^{\mu\nu} F_{\mu\nu}/4$ and $\mathcal{G} = -\tilde{F}^{\mu\nu} F_{\mu\nu}/4$ where $\tilde{F}^{\mu\nu} = \frac{1}{2} \epsilon^{\mu\nu\alpha\beta} F_{\alpha\beta}$. The terms \mathcal{L}_{2n} correspond diagrammatically to one-loop $2n$ -photon scattering amplitudes,

$$\mathcal{L}_{\text{HE}} \sim \text{[diagram 1]} + \text{[diagram 2]} + \dots \quad (3)$$

For the $2 \rightarrow 2$ process of two photons scattering off each other, the total unpolarised photon-photon scattering cross section is [61],

$$\begin{aligned} \sigma &= \frac{973\alpha^4}{10125\pi} \left(\frac{\omega_*}{m_e}\right)^6 \frac{1}{m_e^2} && (\omega_* \ll m_e), \\ \sigma &= 4.7 \frac{\alpha^4}{\omega_*^2} && (\omega_* \gg m_e). \end{aligned} \quad (4)$$

where ω_* is the photon energy in the centre-of-momentum frame (i.e. $\omega_*^2 = (k_1 + k_2)^2/4$ for incoming momenta k_1^μ and k_2^μ). The total cross-section peaks at $\omega_* = 1.5m_e$ [62] i.e. $\omega_* \approx 0.75 \text{ MeV}$, but there are currently no lab-based photon sources with a high enough flux at this energy to see real photon-photon scattering in experiment. If two photons are replaced with couplings to a coherent electromagnetic field, the cross-section can be enhanced by the field strength squared. By using the strongest terrestrial fields, which are produced by focussing optical beams from high-power laser systems, one can compensate for the small value of the cross-section for free photons at these energies $\sigma \sim 10^{-64} \text{ cm}^2$. Another way to enhance photon-photon scattering is to combine optical laser beams with probe photons of a higher energy, such as from a focussed XFEL, which gives a centre-of-mass energy $\omega_* \sim 100 \text{ eV}$ and the cross section $\sigma \sim 10^{-53} \text{ cm}^2$. (For reviews of XFEL theory and facilities see e.g. [63–67].) The combination of optical and XFEL beams has attracted the interest of several groups investigating photon scattering signals in this setup (see e.g [14, 16, 26, 40, 53, 54, 56, 68–78]).

The collision of the pulses can be formulated as a scattering problem, see e.g. [79], with total amplitude

$$S_{\text{fi}} = -i \int d^4x \mathcal{L}_{\text{HE}}. \quad (5)$$

¹ Throughout we use units where $\hbar = c = \epsilon_0 = 1$.

Here, \mathcal{L}_{HE} is the weak-field expansion of the Heisenberg-Euler Lagrangian Eq. (2) and we include terms up to 6-photon scattering. The total EM field can be written as a sum of the colliding and signal fields,

$$F^{\mu\nu}(x) = F_x^{\mu\nu}(x) + F_1^{\mu\nu}(x) + F_2^{\mu\nu}(x) + F_\gamma^{\mu\nu}(x), \quad (6)$$

where F_x is the x-ray probe field, $F_{1,2}$ are the optical pump fields, and F_γ is the signal. When inserted into the amplitude Eq. (5), a large number of scattering channels arise. However, since the x-ray pulse is produced by an XFEL, which typically has field strengths $F_x \ll F_{1,2}$, for the processes of interest the scattering amplitude can be well-approximated by linearising in the x-ray field and the signal, which is also assumed much smaller than the other fields. One can write this linearised amplitude as

$$S_{\text{fi}} \approx \underbrace{S_{12} + S_{11} + S_{22}}_{\text{4-photon}} + \underbrace{S_{1122} + S_{1222} + S_{1112}}_{\text{6-photon}}, \quad (7)$$

where the subscripts indicate the couplings to the pump fields $F_{1,2}$.

The probe and pump fields are taken to be linearly polarised Gaussian focussed pulses in the paraxial approximation, allowing the tensor structure to be separated from the spacetime dependence:

$$F_j^{\mu\nu}(x) = \frac{1}{\omega_j} (k_j^\mu \varepsilon_j^\nu - k_j^\nu \varepsilon_j^\mu) E_j(x), \quad (8)$$

with wavevectors k_j^μ , polarisation vectors ε_j^μ and field profiles E_j for $j \in \{x, 1, 2\}$. (The field profile of the signal photon is similarly defined, but with a plane wave electric field, see appendix A for details.) The scattering channels in Eq. (7) can then be expressed as

$$S_{1^{a_2}b} = T_{ab} \int d^4x E_x(x) E_1^a(x) E_2^b(x) E_\gamma(x), \quad (9)$$

where T_{ab} depends purely on the tensor structures of each of the fields, and a and b denote the number of powers of the fields $E_1(x)$ and $E_2(x)$ involved in the interaction channel, respectively. Thus, S_{12} , S_{11} , and S_{22} in Eq. (7) give the leading-order (LO) 4-photon scattering contribution, while S_{1122} , S_{1112} , and S_{1222} give the next-to-leading order (NLO) 6-photon scattering contribution.

Since the collision is between travelling waves, which have positive and negative frequency components, each of the scattering channels can be decomposed into further sub-channels with different numbers of photons being absorbed from or emitted into the pump fields. For example, we can write

$$E_j(x) = \sum_{\delta_j} E_j^{(\delta_j)}(x) e^{i\delta_j k_j \cdot x},$$

with $\delta_j \in \{-1, 1\}$. To understand the approximate kinematics one can consider the monochromatic limit, which physically corresponds to infinitely long pulses and zero focussing, where $E_j^{(\delta_j)}(x)$ becomes a constant. Then Eq.

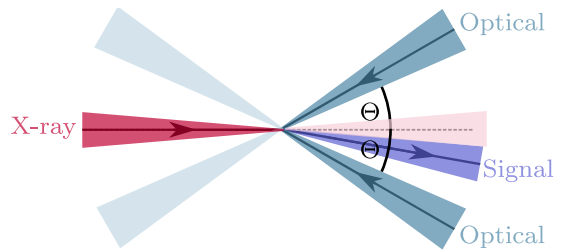


FIG. 1. Schematic of planar three-beam collision. An x-ray beam collides with two optical beams which are at angles Θ and $-\Theta$ from the counter-propagating direction. (Faint colours show the trajectory of the beams after the collision.)

(9) suggests that channel $S_{1^{a_2}b}$ supports scattering with momentum-conservation of the form

$$\delta_x k_x + \underbrace{\delta_1 k_1 + \dots + \delta_{1'} k_{1'}}_{a \text{ terms}} + \underbrace{\delta_2 k_2 + \dots + \delta_{2'} k_{2'}}_{b \text{ terms}} + k_\gamma = 0, \quad (10)$$

where the δ terms can take any possible allowed combination, $k_{j'} = k_j$ in the monochromatic limit but in general $k_{j'} \neq k_j$ in a focussed pulse with finite duration. Then the most interesting scattering channels are those for which the scattered photon is on-shell, i.e. $k_\gamma \cdot k_\gamma = 0$, and hence can reach the detector.

The number of scattered photons N_γ can be calculated in the usual way by mod-squaring the amplitude and integrating over the scattered photon momentum. This can be reformulated as a differential number of photons:

$$\frac{d^3 N_\gamma^{\parallel, \perp}}{d\omega_\gamma d\theta_\gamma d\phi_\gamma} = V^2 \frac{\omega_\gamma^2 \sin \theta_\gamma}{(2\pi)^3} |S_{\text{fi}}(\omega_\gamma, \theta_\gamma, \phi_\gamma, \varepsilon_\gamma^{\parallel, \perp})|^2, \quad (11)$$

where V is a volumetric normalisation factor, the amplitude S_{fi} has now been written explicitly as a function of parameters of the scattered photon, with frequency $\omega_\gamma = k_\gamma^0$ and polarisation basis $\varepsilon_{\parallel, \perp}$ to be later defined. The solid angle co-ordinates $\theta_\gamma, \phi_\gamma$ are defined with respect to the x-ray propagation direction (corresponding to $\theta_\gamma = 0$). The total number of signal photons is then,

$$N_\gamma = N_\gamma^\parallel + N_\gamma^\perp. \quad (12)$$

III. COLLISION GEOMETRY AND KINEMATICS

We consider a planar three-beam configuration where two optical pump fields, which are chosen to have the same form, collide with an XFEL probe field at an angle Θ from head-on and with each other at an angle 2Θ as depicted in Fig. (1). The x-ray propagates down the z axis and the wavevectors are,

$$\begin{aligned} k_x^\mu &= \omega_x (1, 0, 0, 1), \\ k_1^\mu(\Theta) &= \omega_0 (1, \sin \Theta, 0, -\cos \Theta) = k_2^\mu(-\Theta), \\ k_\gamma^\mu &= \omega_\gamma (1, \sin \theta_\gamma \cos \phi_\gamma, \sin \theta_\gamma \sin \phi_\gamma, \cos \theta_\gamma). \end{aligned} \quad (13)$$

For each wavevector one can form a corresponding transverse polarisation basis $\{\alpha_i^\mu, \beta_i^\mu\}$ ($i = \{x, 1, 2\}$), where $k_i \cdot \alpha_i = k_i \cdot \beta_i = \alpha_i \cdot \beta_i = 0$ and $\alpha_i \cdot \alpha_i = \beta_i \cdot \beta_i = -1$. The basis polarisation vectors for the XFEL beam are,

$$\alpha_x^\mu = (0, 1, 0, 0), \quad \beta_x^\mu = (0, 0, 1, 0), \quad (14)$$

such that a general linear polarisation state is,

$$\varepsilon_x^\mu(\psi_x) = (\cos \psi_x) \alpha_x^\mu + (\sin \psi_x) \beta_x^\mu. \quad (15)$$

The corresponding orthonormal polarisation state is:

$$\bar{\varepsilon}_x^\mu(\psi_x) = (\sin \psi_x) \alpha_x^\mu - (\cos \psi_x) \beta_x^\mu. \quad (16)$$

The angle ψ_x defines the polarisation plane of the x-ray beam and will be important in maximising e.g. the number of polarisation-flipped photons. The basis polarisation states for the optical beams are, for $k_1^\mu(\Theta)$,

$$\alpha_1^\mu = (0, \cos \Theta, 0, \sin \Theta), \quad \beta_1^\mu = (0, 0, 1, 0), \quad (17)$$

and for $k_2^\mu(\Theta)$,

$$\alpha_2^\mu = (0, \cos \Theta, 0, -\sin \Theta), \quad \beta_2^\mu = (0, 0, 1, 0). \quad (18)$$

Note that $\beta_x^\mu = \beta_1^\mu = \beta_2^\mu$ as the planar geometry ensures there is a common orthogonal direction normal to the interaction plane. As with the XFEL beam, it is convenient to parameterise the general linear polarisation states of the optical beams through angles ψ_1 and ψ_2 ,

$$\varepsilon_j^\mu(\psi_j) = (\cos \psi_j) \alpha_j^\mu + (\sin \psi_j) \beta_j^\mu, \quad (19)$$

for $j \in \{1, 2\}$. The polarisation vector of the signal photon, ε_γ^μ is defined as,

$$\varepsilon_\gamma^\mu = e^\mu - \frac{e \cdot k_\gamma}{k \cdot k_\gamma} k^\mu, \quad (20)$$

where e^μ is a polarisation direction and k^μ is an arbitrary light-like reference vector. With this definition the signal photon satisfies $k_\gamma \cdot \varepsilon_\gamma = 0$ by construction. Without loss of generality we choose the light-like reference vector as $k^\mu = k_1^\mu$. We will be interested in exploring vacuum birefringence effects, which are microscopically described by polarisation flip of the probe photon from the initial polarisation state to the orthonormal state. Thus, *parallel polarised* signal photons are defined as non-flipped photons with $e^\mu = \varepsilon_x^\mu$,

$$\varepsilon_\gamma^{\parallel\mu}(\psi_x) \equiv \varepsilon_x^\mu(\psi_x) - \frac{k_\gamma \cdot \varepsilon_x(\psi_x)}{k_1 \cdot k_\gamma} k_1^\mu, \quad (21)$$

and *perpendicular polarised* signal photons are those where the polarisation has flipped $e^\mu = \bar{\varepsilon}_x^\mu$,

$$\varepsilon_\gamma^{\perp\mu}(\psi_x) \equiv \bar{\varepsilon}_x^\mu(\psi_x) - \frac{k_\gamma \cdot \bar{\varepsilon}_x(\psi_x)}{k_1 \cdot k_\gamma} k_1^\mu. \quad (22)$$

The scattering channels that are of most interest are the elastic channels that allow for an on-shell photon to

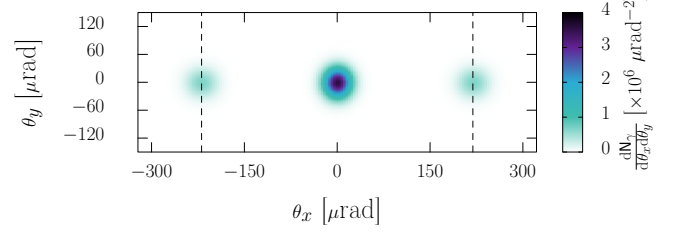


FIG. 2. Differential number of signal photons $\frac{dN_\gamma}{d\theta_x d\theta_y}$ in three-beam configuration using EU.XFEL SASE parameters (Tab. (I)) with $f^\# = 1$ optical focussing and x-ray beam waist $w_x = 4 \mu\text{m}$. Collision angle is $\Theta = 45^\circ$ and x-ray and optical beams have a relative polarisation of $\Delta\psi = \pi/2$. The angles θ_x and θ_y are the scattering angles of the photons inside and out of the interaction plane, respectively, see Eq. (24). Dashed vertical lines are at Bragg peak locations, Eq. (25).

be scattered out of the main background of the XFEL beam. From the general momentum conservation equation in Eq. (10), these channels have $\delta_1 = -\delta_2$ for the LO process of 4-photon scattering and also $\delta_{1'} = -\delta_{2'}$ for the NLO process of 6-photon scattering. Using the specific set-up in Eq. (13), this corresponds to a photon scattered via $2n$ -photon scattering with a momentum

$$k_\gamma^\mu = k_x^\mu \pm (n-1)[k_1^\mu(\Theta) - k_2^\mu(\Theta)]. \quad (23)$$

Although $k_\gamma \cdot k_\gamma \neq 0$, the beams are also not monochromatic. If one allows for a finite bandwidth by replacing $k_\gamma \rightarrow k_\gamma + \Delta$, where the bandwidth Δ is the momentum difference due to taking momenta from three pulses with finite bandwidths, then it follows that the condition $k_\gamma \cdot k_\gamma = 0$ implies that:

$$k_x \cdot \Delta - (n-1)^2 k_1 \cdot k_2 \pm (n-1) \Delta \cdot (k_1 - k_2) + \frac{1}{2} \Delta^2 = 0,$$

where $k_{1,2} \equiv k_{1,2}(\Theta)$. Since the x-ray frequency is $\sim O(10^5)$ times larger than the optical frequency, the requirement on the bandwidth Δ to satisfy the on-shell condition for the scattered photon is easily fulfilled. To parameterise the small scattering angles of the x-ray photons it will also be useful to define the angles $\theta_x = \sin \theta_\gamma \cos \phi_\gamma$ and $\theta_y = \sin \theta_\gamma \sin \phi_\gamma$, such that the signal photon is parameterised by

$$k_\gamma^\mu = \omega_\gamma (1, \theta_x, \theta_y, \sqrt{1 - \theta_x^2 - \theta_y^2}), \quad (24)$$

with the requirement that $\theta_{x,y} \ll 1$.

The scattering channels S_{11} and S_{22} in Eq. (7) correspond to the case that a photon is absorbed and emitted to the same beam, which by energy momentum conservation gives $k_\gamma^\mu \approx k_x^\mu$, (where the \approx sign indicates some allowance for a small spread of momenta due to finite bandwidth effects as explained in the previous paragraph). For these channels the signal photons receive no lateral momentum kick and peak around $\theta_\gamma \approx 0$, along

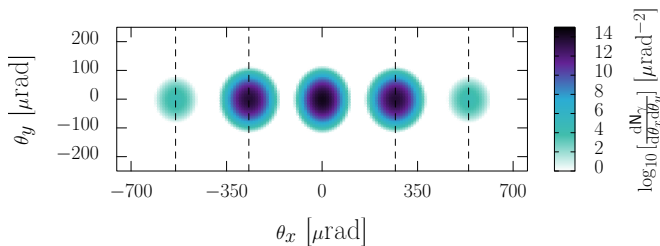


FIG. 3. Logarithmic differential number of signal photons $\log_{10} [dN_\gamma/d\theta_x d\theta_y]$ in three-beam configuration using future SASE parameters (Tab. (I)) with $f^\# = 2$ optical focussing and x-ray beam waist $w_x = 2 \mu\text{m}$. Collision angle is $\Theta = 63^\circ$ and x-ray and optical beams have polarisation $\psi_x = \psi_0 = 0$. Dashed vertical lines are at Bragg peak locations, Eq. (25).

the propagation direction of the probe XFEL beam. Instead, the main interest in the three-beam configuration is in the S_{12} and S_{1122} , channels of Eq. (7) which includes absorption of photons from one optical beam and emission to the other. This produces Bragg side-peaks outside of the emission cone of the XFEL probe beam, centred around $\theta_x \approx \theta_{B,2n} \ll 1$ where,

$$\theta_{B,2n} = 2(n-1) \frac{\omega_0}{\omega_x} \sin \Theta. \quad (25)$$

An example of the distribution of scattered photons for *currently attainable* parameters is shown in Fig. (2). Only two side-peaks are visible, corresponding to 4-photon scattering and $n = 2$ in Eq. (23). At the level of the probability, the coupling to each optical field scales as $E_j^2 \ll 1$ (recall the fields are normalised by the Schwinger critical field strength) and since 6-photon scattering has two extra vertices coupled to optical fields compared with 4-photon scattering, the 6-photon scattering signal is very weak. By momentum conservation in Eq. (23) with $n = 3$ there are two further Bragg side peaks and these are demonstrated in Fig. (3) on a logarithmic plot with *future parameters* for the optical beam. (See Sec. V below for more details on the parameters used.)

IV. DETERMINATION OF FUNDAMENTAL LOW-ENERGY CONSTANTS

First we present analytical results that link the number of polarised and unpolarised scattered photons to the fundamental low-energy constants in Eq. (2). To simplify the analysis we set the polarisation plane of the optical beams to be equal, $\psi_1 = \psi_2 = \psi_0$. Then only two polarisation angles remain: ψ_x for the x-ray polarisation plane and ψ_0 for the optical polarisation plane. We can obtain more manageable expressions for the number of signal photons by considering an expansion of the amplitudes in Eq. (11) for $\theta_x \ll 1$, or equivalently by taking $\theta_\gamma \ll 1$ (see Eq. (24)). In fact, expanding only the *tensor struc-*

ture, i.e. T_{ab} in Eq. (9), one finds that the parallel and perpendicular amplitudes can be expressed as

$$\lim_{\theta_\gamma \rightarrow 0} S_{fi}(\omega_\gamma, \theta_\gamma, \phi_\gamma, \varepsilon_\gamma^{\parallel, \perp}) \approx g_{\parallel, \perp} G + h_{\parallel, \perp} H, \quad (26)$$

where g_{\parallel} , g_{\perp} , h_{\parallel} , and h_{\perp} depend only on the $c_{2n,j}$ and the initial beam polarisations, ψ_x and ψ_0 . Explicitly:

$$\begin{aligned} g_{\parallel} &= c_4^+ + 2c_4^- \cos[2(\psi_x - \psi_0)], \\ g_{\perp} &= -2c_4^- \sin[2(\psi_x - \psi_0)], \\ h_{\parallel} &= (4c_6^+ + c_6^-) \cos(2\psi_x) + 6c_6^- \cos[2(\psi_x - 2\psi_0)] \\ &\quad + 2(4c_6^+ + c_6^-) \cos(2\psi_0), \\ h_{\perp} &= (4c_6^+ + c_6^-) \sin(2\psi_x) + 6c_6^- \sin[2(\psi_x - 2\psi_0)], \end{aligned} \quad (27)$$

where $c_4^+ = c_{4,1} + c_{4,2}$, $c_4^- = c_{4,1} - c_{4,2}$ and $c_6^+ = c_{6,1} + c_{6,2}$, $c_6^- = c_{6,1} - c_{6,2}$. The functions G and H contain all of the spacetime dependent information

$$\begin{aligned} G &= 4 \cos^4 \left(\frac{\Theta}{2} \right) \int d^4x E_x(x) E_\gamma(x) [E_1(x) + E_2(x)]^2, \\ H &= -16 \sin^2 \left(\frac{\Theta}{2} \right) \cos^6 \left(\frac{\Theta}{2} \right) \\ &\quad \times \int d^4x E_x(x) E_1(x) E_2(x) E_\gamma(x) [E_1(x) + E_2(x)]^2, \end{aligned} \quad (28)$$

and, in general, $G \gg H$, since the electric fields are normalised by the critical field. We note here the different dependence of the integral prefactors in G and H on the collision angle, Θ . On the interval $0 < \Theta < \pi/2$, the prefactor of G is a monotonically decreasing function of Θ , with a maximum at $\Theta = 0$. Conversely, the prefactor of H peaks around $\Theta = 60^\circ$, and vanishes for $\Theta = 0$. This emphasises the fact that the NLO contribution is heavily suppressed in a head-on two-beam collision, and indicates a preferred geometry for the three-beam NLO interaction. Later numerical investigation will confirm the NLO signal peaks at $\Theta \approx 60^\circ$.

Consider now the (differential) number of photons scattered into each of the polarisation modes, Eq. (11). With the tensor structure expanded as before, to leading order in $\theta_\gamma \ll 1$, these will take the form,

$$\begin{aligned} \frac{d^3 N_\gamma^{\parallel, \perp}}{d\omega_\gamma d\theta_\gamma d\phi_\gamma} &\approx \frac{\theta_\gamma}{(2\pi)^3} \left[g_{\parallel, \perp}^2 |G|^2 + h_{\parallel, \perp}^2 |H|^2 \right. \\ &\quad \left. + 2|g_{\parallel, \perp} h_{\parallel, \perp}| \Re \epsilon(HG^\dagger) \right]. \end{aligned} \quad (29)$$

These terms contain a dominant contribution from the LO 4-photon interaction, $\propto |G|^2$, a term which depends only on the NLO 6-photon interaction, $\propto |H|^2$, and an interference term which mixes the LO and NLO contributions, $\propto \Re \epsilon(HG^\dagger)$. Since, in general, $G \gg H$, any kinematic region in which the contributions from the LO and NLO diagrams overlap will be dominated by the LO process. We first concentrate on determination of the fundamental low-energy constants of LO scattering.

Fundamental constants of 4-photon scattering

Due to the additional suppression of NLO scattering by powers of the critical field, in detector regions where the contributions from LO and NLO scattering overlap the NLO terms in Eq. (29) can be neglected, giving the simple expressions,

$$\begin{aligned} N_\gamma^\parallel &\approx [c_{4,1} + c_{4,2} + (c_{4,1} - c_{4,2}) \cos(2\Delta\psi)]^2 \mathcal{I}_G, \\ N_\gamma^\perp &\approx [(c_{4,1} - c_{4,2}) \sin(2\Delta\psi)]^2 \mathcal{I}_G, \\ N_\gamma &\approx 2 [c_{4,1}^2 + c_{4,2}^2 + (c_{4,1}^2 - c_{4,2}^2) \cos(2\Delta\psi)] \mathcal{I}_G. \end{aligned} \quad (30)$$

The function \mathcal{I}_G contains all of the spacetime structure and integrations which will be strongly depend on the experimental pulse parameters and shot-to-shot fluctuations. The field-independent pre-factors of \mathcal{I}_G coincide with known scaling laws found for the case of a two-beam head-on collision, see for example [56], and depend only on the 4-photon low-energy constants [80],

$$c_{4,1} = 4 \left(1 + \frac{40}{9} \frac{\alpha}{\pi} \right), \quad c_{4,2} = 7 \left(1 + \frac{1315}{252} \frac{\alpha}{\pi} \right), \quad (31)$$

and the relative polarisation of the x-ray and optical beams $\Delta\psi = \psi_x - \psi_0$. When $\Delta\psi = \pi/4$, N_γ^\perp takes its maximum value of $N_\gamma^\perp \approx (c_{4,1} - c_{4,2})^2 \mathcal{I}_G$; when $\Delta\psi = \pi/2$, N_γ^\parallel and N_γ take their maximum values $N_\gamma^\parallel \approx N_\gamma \approx (2c_{4,2})^2 \mathcal{I}_G$. There are two different types of measurement that can be performed to determine the fundamental low-energy constants $c_{4,1}$ and $c_{4,2}$.

i) *Polarisation-sensitive* measurement of the number of photons at a fixed angle of polarisation of the XFEL beam. In this case, $\Delta\psi$ is fixed and forming the ratio of N_γ^\parallel to N_γ^\perp , we see:

$$\frac{N_\gamma^\perp}{N_\gamma^\parallel} \approx \left(\frac{(c_{4,1} - c_{4,2}) \sin(2\Delta\psi)}{c_{4,1} + c_{4,2} + (c_{4,1} - c_{4,2}) \cos(2\Delta\psi)} \right)^2, \quad (32)$$

which is independent of \mathcal{I}_G and not effected by experimental factors such as the field-strengths, space-time overlap, or collision angle Θ of the three beams.

ii) *Polarisation-insensitive* measurement of just the number of scattered photons N_γ at two different angles of polarisation of the XFEL beam. In this case, the two angles of polarisation correspond to $\Delta\psi$ with a photon count $N_\gamma(\Delta\psi)$ and $\Delta\psi'$ with a photon count $N_\gamma(\Delta\psi')$, with the condition $\Delta\psi' \neq \Delta\psi$. The ratio of these two measurements would also be independent of \mathcal{I}_G ,

$$\frac{N_\gamma(\Delta\psi)}{N_\gamma(\Delta\psi')} = \frac{c_{4,1}^2 + c_{4,2}^2 + (c_{4,1}^2 - c_{4,2}^2) \cos(2\Delta\psi)}{c_{4,1}^2 + c_{4,2}^2 + (c_{4,1}^2 - c_{4,2}^2) \cos(2\Delta\psi')}. \quad (33)$$

These two routes to determining the fundamental low-energy constants $c_{4,1}$ and $c_{4,2}$ have been outlined in the literature for the two-beam case [81]. However, a clear advantage of the three-beam set-up is that the photons

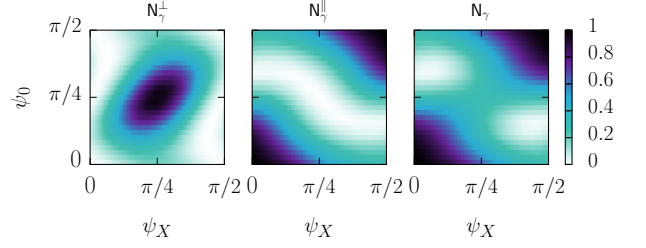


FIG. 4. Polarisation dependence of NLO photon-photon scattering. Polarisation plane of x-ray beam defined by angle ψ_x , see Eq. (15), and polarisation plane of optical lasers defined by $\psi_1 = \psi_2 = \psi_0$, see Eq. (19). Shown are the space-time independent pre-factors of N_γ^\parallel (left-hand plot) and N_γ^\perp (middle plot), given by Eq. (34), and $N_\gamma = N_\gamma^\parallel + N_\gamma^\perp$ (right-hand plot). Each plot has been normalised to a maximum of unity and Eq. (35) has been used.

are scattered into side-peaks and hence are spatially separated from the large x-ray background from the probe XFEL beam. This may prove to be more attractive experimentally than modifying the XFEL beam with advanced techniques such as the shadow technique [56].

A further advantage is the choice of XFEL beam mode. X-ray polarimetry, for example using quasi-channel-cut crystals, can set a strict bound on the allowable bandwidth $\Delta\omega_x$ of the x-ray pulse to the order of $\mathcal{O}(100 \text{ meV})$ [82]. If a measurement requires a high level of x-ray polarimetry this limits the mode of the XFEL beam to use a low-bandwidth option such as self-seeding. However, if polarisation-*insensitive* measurements can be used, such as suggested by the three-beam configuration, there is no strict requirement on the x-ray bandwidth and one can use alternative x-ray modes that offer larger numbers of photons per pulse, such as SASE [59, 60]. Since the total number of signal photons is directly proportional to the number of probe x-ray photons using e.g. the SASE mode can lead to a significant increase in the signal versus a polarisation-sensitive measurement.

Fundamental constants of 6-photon scattering

A highlight of the three-beam configuration is that $2n$ -photon scattering is separated into different side-peaks for different n , see Eq. (25). If the NLO 6-photon side-peak is sufficiently separated from the LO side-peak such that we can neglect the signal from the LO interaction, we find

$$\begin{aligned} N_\gamma^\parallel &\approx [(3c_{6,1} + c_{6,2}) \cos(2\psi_x) + 2(3c_{6,1} + c_{6,2}) \cos(2\psi_0) \\ &\quad + 3(c_{6,1} - c_{6,2}) \cos(2(\psi_x - 2\psi_0))]^2 \mathcal{I}_H, \\ N_\gamma^\perp &\approx [(3c_{6,1} + c_{6,2}) \sin(2\psi_x) \\ &\quad + 3(c_{6,1} - c_{6,2}) \sin(2(\psi_x - 2\psi_0))]^2 \mathcal{I}_H, \end{aligned} \quad (34)$$

and the spacetime dependence can be factorised into the integral \mathcal{I}_H . Just as in the LO case Eq. (32), we can form

the ratio of polarised photons to arrive at a quantity that is relatively insensitive to shot-to-shot variations.

Alongside the 6-photon fundamental low-energy constants [80],

$$c_{6,1} = 8 \left(1 + \frac{8533 \alpha}{1440 \pi} \right), \quad c_{6,2} = 13 \left(1 + \frac{3787 \alpha}{585 \pi} \right), \quad (35)$$

the number of signal photons due to the NLO interaction depends explicitly on the polarisation angles ψ_x and ψ_0 , rather than just their difference as was the case for the LO interaction Eq. (30). The dependence on the polarisation angles is illustrated in Fig. (4). The reason for this different dependency on the polarisation is due to the configuration of colliding three beams. For the side-peaks, the LO process of 4-photon scattering has a different optical beam connected to the two ‘pump’ vertices, whereas for the NLO process of 6-photon scattering the four ‘pump’ vertices involve the same optical beam being connected to two vertices. This has a restrictive effect on the NLO tensor structure which makes it more sensitive to the beam polarisations.

From Fig. (4) it can be seen that the number of perpendicular-polarised photons N_γ^\perp is maximised when $\psi_x = \psi_0 = \pi/4$, but, with this same choice, the number of parallel-polarised photons N_γ^\parallel goes to zero. Likewise, the number of parallel-polarised photons or total number of photons are maximised when $\psi_x = \psi_0 = 0$ or $\pi/2$, where the number of perpendicular-polarised photons N_\perp falls to zero. Making use of the partial symmetry between ψ_x and ψ_0 , we simplify the analysis by choosing $\psi_x = \psi_0 = \psi$. Using Eq. (34), we find

$$\begin{aligned} N_\gamma^\parallel \Big|_{\psi_x=\psi_0=\psi} &\approx 144 c_{6,1}^2 \cos^2(2\psi) \mathcal{I}_H, \\ N_\gamma^\perp \Big|_{\psi_x=\psi_0=\psi} &\approx 16 c_{6,2}^2 \sin^2(2\psi) \mathcal{I}_H, \\ N_\gamma \Big|_{\psi_x=\psi_0=\psi} &\approx 8 (9 c_{6,1}^2 + c_{6,2}^2 + (9 c_{6,1}^2 - c_{6,2}^2) \cos(4\psi)) \mathcal{I}_H. \end{aligned} \quad (36)$$

This also gives a simple ratio,

$$\frac{N_\gamma^\perp}{N_\gamma^\parallel} \Big|_{\psi_x=\psi_0=\psi} \approx \frac{c_{6,2}^2}{9 c_{6,1}^2} \tan^2(2\psi). \quad (37)$$

V. NUMERICAL RESULTS

In this section, we present numerical results for the number of scattered photons for two different sets of experimental parameters. We consider a *currently attainable* case which could be sufficient to measure the LO process of 4-photon scattering and a *future parameters* case which would allow access to the NLO process of 6-photon scattering. Measurement of the NLO process of 6-photon scattering is currently beyond experimental reach, but would be aided by having a more intense optical laser, higher brilliance XFEL beam, or collisions at a higher repetition rate. The numerical results also act as a test of the analytically-derived expressions relating

the fundamental low-energy constants to numbers of polarised and unpolarised scattered photons.

Currently attainable parameters

For the currently-attainable XFEL beam, technology is assumed that is capable of offering hard x-rays with energy $\omega_x \sim \mathcal{O}(10 \text{ keV})$ and numbers of photons per pulse $N_x \sim \mathcal{O}(10^{11} - 10^{12})$. The energy requirement ensures that the photon-photon cross section is enhanced relative to an all-optical configuration while the number of photons per pulse ensures that the number of signal photons, N_γ , which scales as $N_\gamma \propto N_x$, is large enough for a significant number of events to be observed. Also important is the availability of both SASE [59, 60] and self-seeded [85, 86] operational modes. For polarisation resolved measurements, the self-seeded injection scheme is the most suitable (i.e. vacuum birefringence experiments), as typical crystal polarimeters have a narrow acceptance bandwidth $\Delta\omega_x$. For polarisation insensitive measurements, one can instead use the SASE mode which provides a larger number of photons per bunch at the expense of a larger bandwidth. For the currently-attainable optical beams, we assume a peak power $P \sim \mathcal{O}(0.1 - 1 \text{ PW})$ and short duration $\tau_0 \sim \mathcal{O}(10 \text{ fs})$. The number of signal photons, N_γ , scales at LO with the optical beam intensity, I , as $N_\gamma \propto I^2$.

Two examples of facilities meeting the above requirements are the European X-ray Free Electron Laser (EU.XFEL) [82, 87] and the SPring-8 Angstrom Compact Free Electron Laser (SACLA) [83, 84]. The EU.XFEL produces coherent pulses with photon energies in the range $8 \text{ keV} \lesssim \omega_x \lesssim 30 \text{ keV}$. These can be combined with the Ti:Sa optical ReLaX laser system installed at the Helmholtz International Beamline for Extreme Fields (HIBEF) [87], offering a total pulse energy of $W = 4.9 \text{ J}$ at a $\tau_0 = 30 \text{ fs}$ duration, corresponding to a peak power $P \approx 200 \text{ TW}$. The waist is given by $w_0 = f^\# \times 1.3 \mu\text{m}$, where $f^\#$ is the f-number of the focussing optics. Assuming that the ReLaX beamline is passed through a 50:50 beamsplitter to produce two optical pulses with energy $W/2 = 2.45 \text{ J}$, for $f^\# = 1$ each pulse can reach an intensity of $I_0 \approx 5.7 \times 10^{21} \text{ Wcm}^{-2}$. The EU.XFEL parameters in Tab. (I) are taken to coincide with those of the proposed BIREF@HIBEF experiment [82]. SACLA offers a similar XFEL capability, providing coherent pulses with photon energies $4 \text{ keV} \lesssim \omega_x \lesssim 15 \text{ keV}$. At SACLA there is also a Ti:Sa optical laser system capable of delivering two $\tau_0 = 25 \text{ fs}$ duration laser pulses with combined total energy $W = 25 \text{ J}$, corresponding to a total peak power $P \approx 1 \text{ PW}$ [83]. Assuming the capability to focus each pulse to a beam waist $w_0 = f^\# \times 1.3 \mu\text{m}$, as for the ReLaX system above, this corresponds to a peak intensity of $I_0 \approx 3.5 \times 10^{22} \text{ Wcm}^{-2}$ per pulse. In the following sections we will evaluate the feasibility of performing photon-photon scattering discovery experiments at both EU.XFEL and SACLA.

	Optical				X-ray (Self-seeded)				X-ray (SASE)			
	λ_0 [μm]	τ_0 [fs]	w_0 [μm]	W [J]	ω_x [keV]	τ_x [fs]	w_x [μm]	N_x	ω_x [keV]	τ_x [fs]	w_x [μm]	N_x
EU.XFEL [82]	0.8	30	$f^\# \times 1.3$	4.9	10	25	0.1 – 10	2×10^{11}	10	25	0.1 – 10	1×10^{12}
SACLA [83, 84]	0.8	25	$f^\# \times 1.3$	25	10	10	0.1 – 10	1×10^{11}	10	10	0.1 – 10	4×10^{11}
Future	0.8	30	$f^\# \times 1.3$	$f^{\#2} \times 4.2 \times 10^3$	10	25	0.1 – 10	2×10^{11}	10	25	0.1 – 10	1×10^{12}

TABLE I. Optical and x-ray pulse parameters used in numerical results. Optical parameters are the wavelength λ_0 , pulse duration τ_0 , beam waist w_0 , focussing f -number $f^\#$, and total available pulse energy W . X-ray parameters are the energy ω_x , pulse duration τ_x , beam waist w_x , and photons per pulse N_x . Pulse duration is defined with respect to the full-width-at-half-maximum value. Beam waist is defined as the value at which the intensity drops to $1/e^2$ of the peak.

Future Parameters

Going beyond the constraints of currently available technology we also consider what sort of signals one may expect at next generation facilities. Our goal is to explore the feasibility of using such a set up to access both the LO and NLO photon-photon scattering contributions. The number of signal photons from the NLO contribution will be proportional to $N_\gamma \propto E_x^2 E_0^8$, such that there is a strong dependence on the field strength of the optical laser pulses. For this reason, we focus on the interaction of a next generation multi-kJ-class high-power laser system with x-ray pulses. Many x-ray free electron laser facilities which provide high-brightness hard x-ray pulses operate with a similar capability to the EUXFEL and so we will use these parameters for the x-ray beam as a demonstrative example. For the optical laser, we consider pulses of 30 fs duration generated from a Ti:Sa laser system and capable of reaching an intensity level of $I_0 \approx 10^{25} \text{ Wcm}^{-2}$. The parameters of such a laser system are outlined in Tab. (I).

A. Background estimation

The number of signal photons per optimal collision of the three beams can reach of the order $N_\gamma \sim \mathcal{O}(10^{-5} - 10^{-1})$ per collision for the ‘currently attainable’ parameters in Tab. (I). The number of x-ray photons per shot is $\sim \mathcal{O}(10^{11} - 10^{12})$. Although the signal is separated from the background in spatial co-ordinate and polarisation, a good understanding of the background is essential in any experiment. Considering the background also allows one to determine suitable values for the remaining free x-ray and optical beam parameters, namely the x-ray photon energy, ω_x , and the x-ray and optical beam waists, w_x and w_0 .

The majority of the XFEL photons will be filtered out by placing the detector at the position of the Bragg side-peaks and ensuring those peaks are a suitable distance from the central peak. Consider a detector a distance $L \sim \mathcal{O}(\text{m})$ down the x-ray propagation axis with a circular exclusion region of radius R , corresponding to an angular cut $\theta_* = \tan^{-1}(R/L)$. Assuming that the detector can measure all signal photons with $\theta_\gamma > \theta_*$, the

total number of signal photons will be,

$$N_{\gamma,*} = \int_{\theta_*}^{\infty} \frac{dN_\gamma}{d\theta_\gamma} d\theta_\gamma. \quad (38)$$

Treating the measurement of the number of scattered photons as Poissonian with a background count per shot of N_γ^{bg} , following [88], the number of optimal shots required to reach a statistical significance of $n\sigma$ using the three-beam scenario is

$$N_{\text{shots}}^{n\sigma} \gtrsim \frac{n^2}{2} \left[(N_{\gamma,*} + N_\gamma^{\text{bg}}) \ln \left(1 + \frac{N_{\gamma,*}}{N_\gamma^{\text{bg}}} \right) - N_{\gamma,*} \right]^{-1}. \quad (39)$$

We identify two potential sources of background for all measurements: the divergence of the x-ray beam, N_x^{bg} , and Compton scattering from impurities in the vacuum chamber, N_C^{bg} . Another source of background, effecting only polarisation sensitive measurements, is due to the polarisation purity of the probe x-ray pulse, N_P^{bg} . The total background is then

$$N_\gamma^{\text{bg}} = N_x^{\text{bg}} + N_C^{\text{bg}} + N_P^{\text{bg}}. \quad (40)$$

The optical elements used to focus the x-ray beam will also impact the number of signal and background photons per shot. Assuming the use of two standard beryllium lenses, one to focus the probe beam and another to focus the signal, each with a 50% transmission, this leads to a total reduction by a factor 0.25 in the number of signal and background photons.

X-ray beam divergence: The biggest potential source of background comes from the divergence of the probe x-ray beam. Since $N_x \gg N_{\gamma,*}$, measurements will be background dominated if even a fraction of a percent of probe photons diverge beyond the detector exclusion region. The number of XFEL photons beyond the angular cut θ_* can be estimated by integrating E_x^2 , given by Eq. (A1), on the detector over time and azimuthal angle:

$$N_x^{\text{bg}} \approx N_x e^{-\sigma_x^{-2} \tan^2 \theta_*}; \quad \sigma_x^2 = \frac{w_x^2}{2L^2} + \frac{1}{2f_x^2 \pi^2} \quad (41)$$

where $f_x = w_x/\lambda_x$ is the focussing f_x -number and $\lambda_x = 2\pi/\omega_x$ is the wavelength of the x-rays. If one demands $N_x^{\text{bg}} \ll N_\gamma$, then:

$$\tan \theta_* \gg \sigma_*, \quad \sigma_* = \sigma_x \left(\ln \frac{N_x}{N_\gamma} \right)^{1/2}. \quad (42)$$

For the XFEL + optical set-up considered here, $\tan \theta_* \approx \theta_*$ and $\sigma_x \approx 1/(f_x \pi \sqrt{2})$. If we choose $\theta_* > C \sigma_x$ for some C to fulfil Eq. (42), then a condition on the angular detector cut is:

$$\theta_* > \frac{C}{f_x \pi \sqrt{2}}. \quad (43)$$

We expect that when the signal is largest, the centre of the Bragg side peaks will be on the detector, $\theta_{B,2n} > \theta_*$, which also implies $\theta_{B,2n} > C \sigma_x$. Using Eq. (25) this gives a condition:

$$w_x > \frac{C \lambda_0}{2\sqrt{2}\pi(n-1)\sin\Theta}. \quad (44)$$

These conditions imply a hierarchy for the associated angles, $\theta_x < \theta_* < \theta_\gamma$. Considering the $C = 10$ standard deviation of an x-ray pulse with $\omega_x = 10$ keV $\implies \lambda_x = 0.12$ nm, the angular cut must satisfy $\theta_* [\mu\text{rad}] > 270 w_x^{-1} [\mu\text{m}]$. Similarly, considering the optical pulse with $\lambda_0 = 0.8 \mu\text{m}$ and a collision angle of $\Theta = 30^\circ$, the condition in Eq. (44) sets a lower bound of $w_x > 1.8 \mu\text{m}$ for the LO contribution with $n = 2$. Thus, a choice of $w_x = 4 \mu\text{m}$ and $\theta_* = 200 \mu\text{rad}$ satisfies the x-ray divergence and Bragg side-peak conditions, and a detector placed $L = 5$ m down the x-ray beamline will measure $N_x^{\text{bg}} \approx 0$ background photons from the x-ray beam divergence outside of the exclusion region, such that we can neglect this contribution to the background.

Compton scattering: Another source of background will be from Compton scattering of x-ray photons and electrons in the interaction vacuum chamber, as in practice a perfect vacuum is not feasible. The interaction geometry of the three-beam setup makes a precise calculation of the background due to Compton scattering a nontrivial task [89]. However, one can estimate an upper bound on this background in the following way. Given an x-ray pulse with N_x photons in a duration τ , the number of scattered photons due to Compton scattering can be estimated as $N_C^{\text{bg}} = \sigma_T n_e N_x \tau$, where $\sigma_T = 6.65 \times 10^{-29} \text{ m}^2$ is the Thomson scattering cross section and n_e is the density of electrons. We assume a vacuum of 10^{-9} torr, corresponding to $n_e \approx 5 \times 10^9 \text{ cm}^{-3}$, which gives $N_C^{\text{bg}} \approx N_x \times 2.5 \times 10^{-18}$. This estimate does not include considerations about the number of these photons which will reach the detectors or the effect of ponderomotive blow out on the electron population, both of which should act to reduce the contribution to the background from Compton scattering (see e.g. [23] for a similar discussion in the context of colliding three optical pulses). Thus, N_C^{bg} can be viewed as an upper bound.

X-ray polarisation purity: For polarisation sensitive measurements we must also consider the effect of the polarisation purity of the probe x-ray beam, $\mathcal{P} = N_x^\perp / N_x$, where N_x^\perp is the number of photons in the probe pulse which are polarised in the orthogonal polarisation mode. An orthogonally polarised photon in the initial beam scattering *without* polarisation flip will contribute a background $N_P^{\text{bg}\perp} \approx \mathcal{P} N_{\gamma,*}^\perp$ to the $N_{\gamma,*}^\perp$ measurement, while

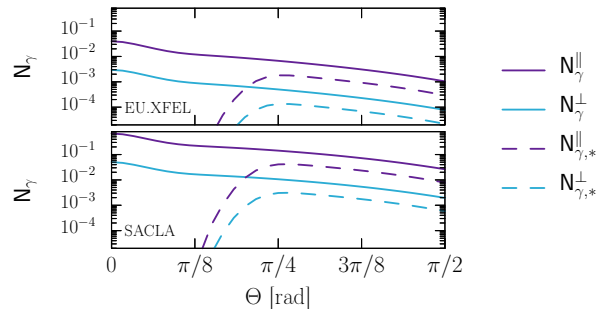


FIG. 5. Number of signal photons vs collision angle Θ using $\omega_x = 10$ keV self-seeded EU.XFEL parameters (upper panel) and SACLA parameters (lower panel). Optical pulses have $f^\# = 1$ focussing, x-ray pulses focussed to $w_x = 4 \mu\text{m}$, and relative polarisation angle is $\Delta\psi = \pi/4$. Plotted is the number of photon N_γ^\parallel scattered into the ‘parallel’ state (purple solid line), the number N_γ^\perp scattered into the ‘perpendicular’ state (blue solid line), and the equivalent photon counts if an angular cut is applied which only accepts photons with emission angles $\theta_x > 200 \mu\text{rad}$ (corresponding dashed lines).

those photons scattering *with* polarisation flip will contribute a background $N_P^{\text{bg}\parallel} \approx \mathcal{P} N_{\gamma,*}^\perp$ to the $N_{\gamma,*}^\parallel$ measurement. While this background could be reduced by using additional polarisers to improve the polarisation purity of the x-ray pulses, these also introduce detrimental effects such as transmission losses and pulse lengthening [76]. We will find, below, that the EU.XFEL polarisation purity of $\mathcal{P} \approx 10^{-6}$ without additional polarisers leads to backgrounds that are sufficiently small [90]. For polarisation insensitive measurements, where only the photon count on the detector is important, the background N_P^{bg} is a component of the signal itself, and so can be neglected.

B. Polarisation-sensitive measurements

1. Currently available technology: 4-photon scattering

Our goal now is to estimate the number of signal photons which could be obtained in a polarisation sensitive measurement using technology currently available at EU.XFEL and SACLA, using Tab. (I). We consider the scattering of $\omega_x = 10$ keV self-seeded photons with optical pulses at $f^\# = 1$ ($w_0 = 1.3 \mu\text{m}$) focussing. The remaining free parameters are $C = 10$, $w_x = 4 \mu\text{m}$ and $\theta_* = 200 \mu\text{rad}$, satisfying the constraints Eq. (42)–(44). The angle between the x-ray and optical polarisation planes is chosen as $\Delta\psi = \pi/4$, maximising the number of x-ray photons scattered into the ‘flipped’ polarisation state, c.f. Eq. (30). The number of signal photons per optimal shot neglecting losses due to x-ray optics is shown in Fig. (5) for both EU.XFEL (upper panel) and SACLA (lower panel) parameters with $f^\# = 1$ focussing of the optical pulses. Choosing an angular cut

$\theta_* = 200 \mu\text{rad}$, the dashed lines in Fig. (5) show the number of parallel ($N_{\gamma,*}^{\parallel}$) and perpendicular ($N_{\gamma,*}^{\perp}$) polarised photons with scattering angles $\theta_\gamma > \theta_*$, peaking at a collision angle $\Theta \approx 45^\circ$ with $N_{\gamma,*}^{\parallel} \approx 1.8 \times 10^{-3}$ and $N_{\gamma,*}^{\perp} \approx 1.3 \times 10^{-4}$ for EU.XFEL parameters and at $\Theta \approx 48^\circ$ with $N_{\gamma,*}^{\parallel} \approx 4.2 \times 10^{-2}$ and $N_{\gamma,*}^{\perp} \approx 3.1 \times 10^{-3}$ for SACLA parameters.

The number of background photons of any polarisation due to Compton scattering is determined as $N_C^{\text{bg}} \approx 5 \times 10^{-7}$ for the EU.XFEL parameters and for $N_C^{\text{bg}} \approx 2.5 \times 10^{-7}$ SACLA parameters. The number of background photons in a *specific* polarisation can be acquired by considering x-ray pulse polarisation purity, $\mathcal{P} = N_x^{\perp}/N_x \approx 10^{-6}$ [90], giving $N_C^{\text{bg}\parallel} = (1 - \mathcal{P})N_C^{\text{bg}}$ for the Compton parallel polarisation background, and $N_C^{\text{bg}\perp} = \mathcal{P}N_C^{\text{bg}}$ for the Compton perpendicular polarisation background. This corresponds to $(N_C^{\text{bg}\parallel}, N_C^{\text{bg}\perp}) = (5 \times 10^{-7}, 5 \times 10^{-13})$ for the EU.XFEL and $(N_C^{\text{bg}\parallel}, N_C^{\text{bg}\perp}) = (2.5 \times 10^{-7}, 2.5 \times 10^{-13})$ for SACLA. For polarisation sensitive measurements we also have to estimate the direct contribution to the background from the polarisation purity. For the total number of x-ray photons per pulse of N_x , there are $N_x^{\perp} = \mathcal{P}N_x$ probe photons in the orthogonal polarisation mode. The contribution to the background from these photons depends on the pulse parameters and configuration. Considering the collision at $\Theta = 45^\circ$ which approximately maximises the signals for photons with $\theta_\gamma > \theta_*$ for EU.XFEL and SACLA parameters, we find the polarisation purity contributes $N_{\mathcal{P}}^{\text{bg}\parallel} \approx 1.3 \times 10^{-10}$ and $N_{\mathcal{P}}^{\text{bg}\perp} \approx 1.8 \times 10^{-9}$ background photons to, respectively, the parallel and perpendicular EU.XFEL measurements, and $N_{\mathcal{P}}^{\text{bg}\parallel} \approx 3.0 \times 10^{-9}$ and $N_{\mathcal{P}}^{\text{bg}\perp} \approx 4.1 \times 10^{-8}$ background photons to the SACLA measurements. Thus, the main contribution to the parallel polarisation background is from Compton scattering, while the polarisation purity of the probe is the dominant background factor of the perpendicular measurement. Including the effect of focussing optics by reducing the signal and background contributions by a factor 0.25, the detected photon counts are given in Tab. (II). Using these in Eq. (39) we can estimate the number of optimal shots which would be required to achieve a statistical significance of 5σ in a polarisation sensitive measurement. For EU.XFEL parameters we find $N_{\text{shots}}^{5\sigma,\parallel} \gtrsim 3.9 \times 10^3$ and $N_{\text{shots}}^{5\sigma,\perp} \gtrsim 3.7 \times 10^4$, while for SACLA parameters we find $N_{\text{shots}}^{5\sigma,\parallel} \gtrsim 1.2 \times 10^2$ and $N_{\text{shots}}^{5\sigma,\perp} \gtrsim 1.6 \times 10^3$. Since the parallel and perpendicular photons can be measured simultaneously in a single shot, the total number of required shots to obtain 5σ significance in both observables will be determined by $N_{\text{shots}}^{5\sigma} \gtrsim \max(N_{\text{shots}}^{5\sigma,\parallel}, N_{\text{shots}}^{5\sigma,\perp})$, which is also shown in Tab. (II).

While we have provided estimates and chosen suitable parameters to minimise the background contributions for idealised shots, we have not taken into account experimental fluctuations. The estimates of the number of

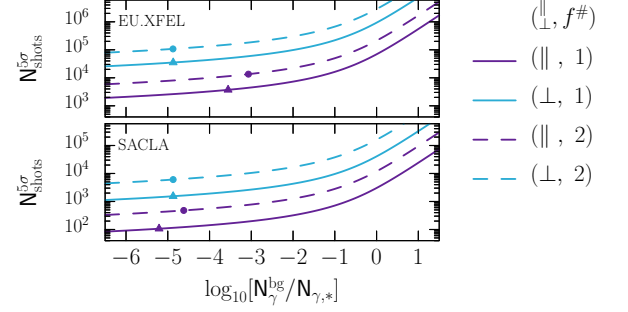


FIG. 6. Estimated number of shots required to achieve 5σ significance as a function of the ratio $N_{\gamma}^{\text{bg}}/N_{\gamma,*}$. X-ray and optical pulse parameters as in Fig. (5) with $\Theta = 45^\circ$. Estimations of number of signal photons held fixed and given by Tab. (II). *Purple solid:* $f^\# = 1$ parallel. *Blue solid:* $f^\# = 1$ perpendicular. *Purple dashed:* $f^\# = 2$ parallel. *Blue dashed:* $f^\# = 2$ perpendicular. The data points correspond to the background estimations in Tab. (II).

shots required for a given $n\sigma$ will be sensitive to the actual background which is measured in each shot. When more factors are taken into account, the level of the background in experiment may take different values than considered here. Therefore, it is useful to understand how the projected number of required shots changes with the background, for the estimated number of signal photons in Tab. (II). In Fig. (6) the number of shots required for a statistical significance of 5σ is calculated according to Eq. (39) as a function of the ratio $N_{\gamma}^{\text{bg}}/N_{\gamma,*}$. Since the number of signal photons in each case is fixed to the estimates in Tab. (II), the increase in $N_{\gamma}^{\text{bg}}/N_{\gamma,*}$ corresponds to an increase in the background. The data points correspond to the background estimations in Tab. (II).

In Sec. IV it was shown that the ratio of polarised scattered photons, $N_{\gamma}^{\perp}/N_{\gamma}^{\parallel}$, is independent of the space-time overlap of the beams. Determining the ratio allows the fundamental QED low-energy constants to be inferred. This conclusion is supported by the numerical result in Fig. (7), which calculates this ratio numerically and finds the same result as the analytical prediction Eq. (31). This also confirms the dependency of the ratio of polarised photons $N_{\gamma}^{\perp}/N_{\gamma}^{\parallel}$ on the angle $\Delta\psi$ between the x-ray and optical polarisation planes from Eq. (32).

In experiment it may be advantageous to increase the x-ray and optical beam-overlap (for example to minimise the effect of beam jitter), which can be achieved by defocussing the optical laser. Since the number of polarisation-flipped photons $N_{\gamma}^{\perp} \propto I_x I_0^2$, where I is the intensity of the corresponding field changing the optical f-number from $f^\# = 1$ to $f^\# = 2$, naively results in the intensity change $I_0 \rightarrow I_0/4$ and the reduction in the number of signal photons by over a magnitude $N_{\gamma}^{\perp} \rightarrow N_{\gamma}^{\perp}/16$. However, if w_x is kept fixed and $w_x > w_0$, the reduction due to the increase in w_0 will be partially compensated by more probe photons being within the foci of the op-

	$f^\#$	$N_{\gamma,*}^\parallel$	$N_\gamma^{\text{bg}\parallel}$	$N_{\gamma,*}^\perp$	$N_\gamma^{\text{bg}\perp}$	$N_{\text{shots}}^{3\sigma}$	$N_{\text{shots}}^{5\sigma}$
EU.XFEL	1	4.5×10^{-4}	1.3×10^{-7}	3.3×10^{-5}	4.5×10^{-10}	1.3×10^4	3.7×10^4
	2	1.5×10^{-4}	1.3×10^{-7}	1.1×10^{-5}	1.5×10^{-10}	4.0×10^5	1.1×10^5
SACLA	1	1.0×10^{-2}	6.3×10^{-8}	7.6×10^{-4}	1.0×10^{-8}	5.8×10^2	1.6×10^3
	2	2.6×10^{-3}	6.3×10^{-8}	1.9×10^{-4}	2.6×10^{-9}	2.3×10^3	6.3×10^3

TABLE II. Estimated number of parallel, $N_{\gamma,*}^\parallel$, and perpendicular, $N_{\gamma,*}^\perp$, polarised signal photons in a polarisation sensitive measurement with associated backgrounds, $N_\gamma^{\text{bg}\parallel}$ and $N_\gamma^{\text{bg}\perp}$. Estimates account for the use of two standard beryllium lenses with 50% transmission to focus the probe and scattered beams. Also shown is the estimated number of shots $N_{\text{shots}}^{\text{ns},\parallel} = \max(N_{\text{shots}}^{\text{ns},\parallel}, N_{\text{shots}}^{\text{ns},\perp})$ required for 3σ and 5σ statistical significance, calculated assuming an optimal collision. Therefore it is an approximate lower bound on the number of shots required as effects such as beam jitter can reduce the number of signal photons.

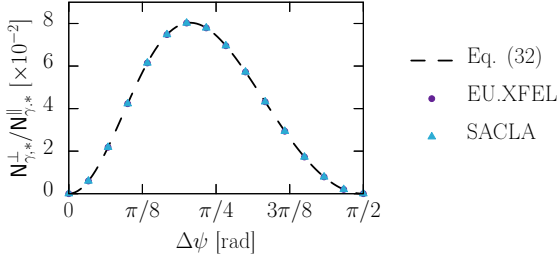


FIG. 7. Ratio of number of signal photons in each polarisation mode $N_{\gamma,*}^\perp / N_{\gamma,*}^\parallel$ vs relative polarisation $\Delta\psi$ for fixed collision angle $\Theta = 45^\circ$, $f^\# = 1$ optical focussing, and $w_x = 4 \mu\text{m}$. *Black line*: analytical result from Eq. (32) with $c_{4,1}$ and $c_{4,2}$ given by Eq. (31). *Purple circles*: Numerically evaluated ratio using EU.XFEL parameters. *Blue triangles*: Numerically evaluated ratio using SACLA parameters.

tical pulses. Fig. (8) shows how the birefringence signal depends on the relative overlap of the x-ray and optical beams, which can be quantified by the ratio w_x/w_0 , using EU.XFEL parameters. Overall, we see for fixed w_x/w_0 , doubling $f^\#$ leads to around an order of magnitude reduction in $N_{\gamma,*}^\perp$. For fixed $f^\#$, going from $w_x/w_0 = 1$ to $w_x/w_0 = 6$ results in around an order of magnitude decrease in the number of scattered photons.

2. Next generation technology: 6-photon scattering

With each power of the electric field strength in \mathcal{L} in Eq. (2) there is also an additional suppression by the critical field strength, E_{cr} . Therefore, the measurable photons mostly originate from the LO process; when attempting to isolate the NLO process, the LO process becomes a source of background. One tool which we can use to aid with separating the contributions is the angular cut on the detector. The Bragg peaks corresponding to the NLO interaction are centered around $\theta_x \approx \theta_{B,6} = 4\omega_0/\omega_x \sin \Theta$, which is twice as far from the origin as the LO Bragg peak, see Eq. (25). Thus, we expect that a larger angular cut (which will turn out to be

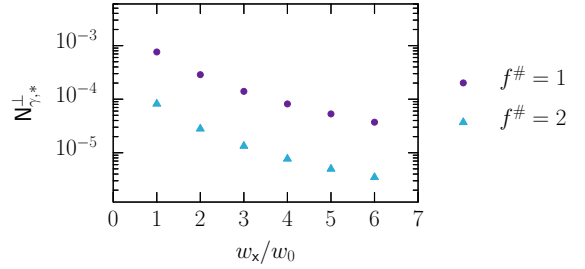


FIG. 8. Dependence of number of perpendicular polarised signal photons $N_{\gamma,*}^\perp$ at collision angle $\Theta = 45^\circ$ on the ratio of the x-ray and optical beam waists w_x/w_0 using EU.XFEL parameters with $f^\# = 1$ (purple circles) and $f^\# = 2$ focussing (blue triangles).

around twice the cut used in the preceding section) can be taken to isolate the signal from the NLO interaction on the detector. This has an additional effect of allowing us to choose a smaller beam waist for the x-ray pulses, w_x , while still ensuring that the background due to its divergence is negligible and the conditions Eq. (41)–(44) are satisfied. Correspondingly, in the following we choose $\theta_* = 450 \mu\text{rad}$ and $w_x = 2 \mu\text{m}$. The remaining parameters for the x-ray and optical lasers are given in Tab. (I), where we choose $f^\# = 2$ focussing for the optical lasers.

Consider now the birefringent signal. To determine the fundamental constants using Eq. (36) for a fixed polarisation angle of the x-ray and optical beams, both the number of parallel-polarised *and* perpendicular-polarised photons must be measured. We saw from Fig. (4) that as the optical and x-ray polarisation plane angle, ψ , is varied, the number of photons scattered into the perpendicular polarisation mode is maximised where the number in the parallel mode vanishes and vice versa. To determine a suitable value for ψ , we pick the value at which the ratio $N_{\gamma,*}^\perp / N_{\gamma,*}^\parallel \rightarrow 1$. From Eq. (37), this occurs when

$$\psi = \psi_* = \begin{cases} \frac{\tan^{-1}\left(\frac{3c_{6,1}}{c_{6,2}}\right)}{2} \approx 30.8^\circ \\ \frac{\pi - \tan^{-1}\left(\frac{3c_{6,1}}{c_{6,2}}\right)}{2} \approx 59.2^\circ \end{cases}, \quad (45)$$

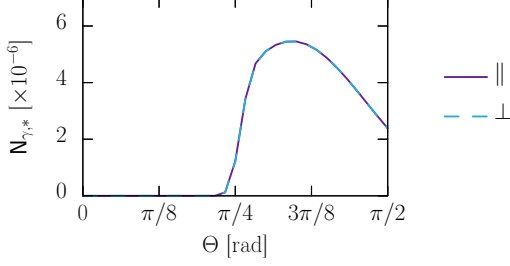


FIG. 9. Number of signal photons vs collision angle Θ from the collision of EUXFEL self-seeded $\omega_x = 10$ keV photons with two future laser pulses. X-ray pulses focussed to $w_x = 4 \mu\text{m}$ and optical pulses focussed with $f^\# = 2$. X-ray and optical pulses have polarisation angle $\psi = \psi_*$, c.f. Eq. (45) at which the number of parallel and perpendicular photons are equal. Plotted is the number of photon N_γ^\parallel scattered into the ‘parallel’ state (purple solid line), the number N_γ^\perp scattered into the ‘perpendicular’ state (blue dashed line) if an angular cut is applied which only accepts photons with emission angles $\theta_x > 450 \mu\text{rad}$ (corresponding dashed lines).

where the approximated values are those obtained using Eq. (35). For other choices of ψ , one of N_γ^\perp or N_γ^\parallel will be smaller, making measurement more difficult. The choice of $\psi = \psi_* = \tan^{-1}(3c_{6,1}/c_{6,2})/2$ is selected for Fig. (9), which shows the number of signal photons in each polarisation mode. The number of parallel polarised photons $N_{\gamma,*}^\parallel$ with $\theta_x > \theta_*$. As expected from our choice of $\psi = \psi_*$, we find that the number of parallel and perpendicular polarised photons coincide, peaking around $\Theta \approx 63^\circ$ with the value $N_{\gamma,*}^\parallel = N_{\gamma,*}^\perp \approx 5.5 \times 10^{-6}$. Following the same analysis as in the preceding section of estimating the background per shot and taking into account the x-ray optics, we find,

$$\frac{N_{\gamma,*}^\parallel}{1.4 \times 10^{-6}} \quad \frac{N_\gamma^{\text{bg}\parallel}}{1.3 \times 10^{-7}} \quad \bigg| \quad \frac{N_{\gamma,*}^\perp}{1.4 \times 10^{-6}} \quad \frac{N_\gamma^{\text{bg}\perp}}{1.5 \times 10^{-12}} \quad (46)$$

which amounts to $N_{\text{shots}}^{5\sigma,\parallel} \gtrsim 7.2 \times 10^6$ and $N_{\text{shots}}^{5\sigma,\perp} \gtrsim 7.1 \times 10^5$. While the number of shots is perhaps prohibitively large for a birefringent measurement to be feasible using the proposed parameters, particularly since the high pulse energy requirement of the optical pulses would likely mean a low repetition rate, we emphasise that the number of signal photons is directly proportional to the number of XFEL photons, N_x . We have considered here a next generation high-power laser combined with an XFEL with currently available technology. Thus, it is possible that advances in XFEL technology could push the birefringent signal to a viable level for detection in an experiment.

Before moving on to consider the polarisation insensitive case we consider how the ratio $N_\gamma^\perp/N_\gamma^\parallel$ varies for the NLO contribution. Choosing the collision angle $\Theta = 63^\circ$ which maximises the birefringent signal of photons with

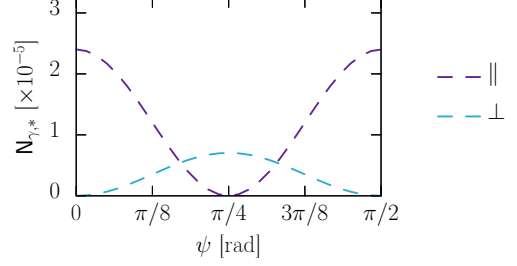


FIG. 10. Dependence of the signal photons $N_{\gamma,*}^{\parallel,\perp}$ on the polarisation ψ for fixed collision angle $\Theta = 63^\circ$. X-ray and optical pulse parameters as in Fig. (9). Plotted is the number of photon N_γ^\parallel scattered into the ‘parallel’ state (purple), and the number N_γ^\perp scattered into the ‘perpendicular’ state (blue), if an angular cut is applied which only accepts photons with emission angles $\theta_x > 450 \mu\text{rad}$.

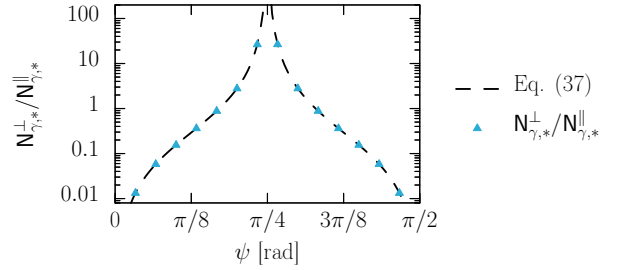


FIG. 11. Ratio of number of photons in each polarisation mode $N_\gamma^\perp/N_\gamma^\parallel$ vs polarisation ψ for fixed collision angle $\Theta = 63^\circ$. X-ray and optical pulse parameters as in Fig. (9). *Black line*: analytical result from Eq. (37) with $c_{6,1}$ and $c_{6,2}$ given by Eq. (35). *Blue triangles*: Numerically evaluated ratio of signal photons with $\theta_\gamma > \theta_*$, $N_{\gamma,*}^\perp/N_{\gamma,*}^\parallel$.

$\theta_x > 450 \mu\text{rad}$ in Fig. (9), we plot in Fig. (11) the ratio Eq. (37) with Eq. (35) (black solid) against the numerically evaluated ratio. We find perfect agreement between the two cases.

C. Polarisation-insensitive measurements

1. Currently available technology: 4-photon scattering

We now consider measurement of the unpolarised process. One advantage of a polarisation insensitive measurement is that the SASE mode of the XFEL can be used, which increases the number of photons per bunch (see Tab. (I)). From Eq. (30) and Eq. (31) it is clear that the total number of signal photons is maximised when the difference in polarisation angle, $\Delta\psi = \pi/2$. In this case the number of perpendicular polarised photons

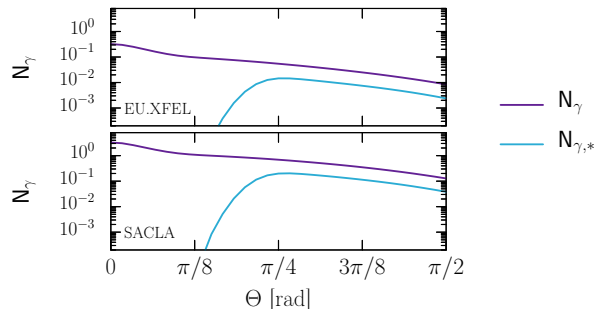


FIG. 12. Number of signal photons vs collision angle Θ in a polarisation insensitive measurement using EUXFEL (upper panel) and SACLA (lower panel) SASE parameters. Optical pulses focussed with $f^\# = 1$ focussing, x-ray pulses focussed to $w_x = 4 \mu\text{m}$, and relative polarisation angle $\Delta\psi = \pi/2$. Plotted is the total number of photons N_γ (purple) and the equivalent photon counts if an angular cut is applied which only accepts photons with emission angles $\theta_x > 200 \mu\text{rad}$ (blue).

drops to zero (see Eq. (30)). The dependence of the total number of signal photons versus the collision angle Θ is shown in Fig. (12) for $f^\# = 1$ focussing with EUXFEL (upper panel) and SACLA (lower panel) SASE parameters. The solid lines show the total number of signal photons with all scattering angles, N_γ , i.e. including those in the central peak (see Fig. (2)). Since the signal photons are purely parallel polarised, the photons in the central peak will of course be indistinguishable from the background probe XFEL photons, and so the dashed lines show the total number of signal photons with angles $\theta_x > 200 \mu\text{rad}$, $N_{\gamma,*}$. This peaks at the collision angle $\Theta \approx 45^\circ$ with $N_{\gamma,*} \approx 1.5 \times 10^{-2}$ for EUXFEL parameters, and $\Theta \approx 48^\circ$ with $N_{\gamma,*} \approx 2.0 \times 10^{-1}$ for SACLA. The combination of the increase in the number of probe photons, N_x , and the use of the polarisation difference $\Delta\psi = \pi/2$ leads to almost an order of magnitude increase in the number of signal photons per shot with comparison to the polarisation sensitive measurements, Fig. (5).

To enable the determination of the experimental values of the 4-photon low-energy constants $c_{4,1}$ and $c_{4,2}$ it is necessary to perform at least two independent measurements. For the polarisation sensitive measurement of Sec. VB 1 these were the number of photons scattered into the parallel and perpendicular polarisation modes. For a polarisation insensitive measurement, where only the total number of signal photons is obtained, the two independent observables must come from measurements at different choices of the relative angle of the XFEL and optical polarisation planes, $\Delta\psi$. How the number of signal photons varies with $\Delta\psi$ for fixed collision angle $\Theta = 45^\circ$ is shown in Fig. (13) for EUXFEL parameters. Unlike in the polarisation sensitive measurement, where the difference in the number of parallel and perpendic-

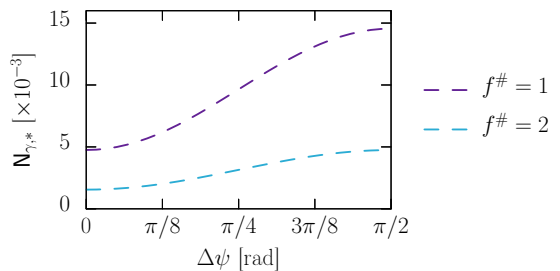


FIG. 13. Dependence of the signal photons $N_{\gamma,*}$ on the relative polarisation $\Delta\psi$ for fixed collision angle $\Theta = 45^\circ$ using EUXFEL SASE parameters. Plotted is the total number of photons $N_{\gamma,*}$ detected if an angular cut is applied which only accepts photons with emission angles $\theta_x > 200 \mu\text{rad}$ for $f^\# = 1$ (purple) and $f^\# = 2$ (blue) focussing of the optical laser.

ular signal photons per shot is over an order of magnitude, the difference between a measurement at $\Delta\psi = 0$ and $\Delta\psi = \pi/2$ is only around a factor of 3. This means that each measurement will require a comparable number of shots to reach a particular statistical significance and, coupled with the higher number of signal photons per shot, the total required shots to determine $c_{4,1}$ and $c_{4,2}$ will be less than in the polarisation sensitive case.

We again wish to estimate the minimum number of shots required to obtain a 5σ statistical significance, $N_{\text{shots}}^{5\sigma}$. With the background from the x-ray divergence $N_x^{\text{bg}} \approx 0$ and the polarisation purity playing no role, the main source of background in the polarisation insensitive measurement will be from Compton scattering, $N_\gamma^{\text{bg}} \approx N_C^{\text{bg}}$, which is estimated as $N_C^{\text{bg}} \approx 2.5 \times 10^{-6}$ for EUXFEL parameters and $N_C^{\text{bg}} \approx 1.0 \times 10^{-6}$ for SACLA parameters. Accounting for the reduction of both the signal and background by the x-ray optics, the number of signal photons for different $\Delta\psi$ measurements and optical focussing are presented in Tab. (III). Taking the independent observables to be the measurements at $\Delta\psi = (\pi/4, \pi/2)$ at $f^\# = 1$ optical focussing, these estimates correspond to $N_{\text{shots}}^{5\sigma, \pi/4} \gtrsim 7.1 \times 10^2$ and $N_{\text{shots}}^{5\sigma, \pi/2} \gtrsim 4.5 \times 10^2$ for EUXFEL parameters, and $N_{\text{shots}}^{5\sigma, \pi/4} \gtrsim 3.5 \times 10^1$ and $N_{\text{shots}}^{5\sigma, \pi/2} \gtrsim 2.2 \times 10^1$ for SACLA parameters. The total number of shots required to measure both observables will be the sum $N_{\text{shots}}^{5\sigma} \gtrsim N_{\text{shots}}^{5\sigma, \pi/4} + N_{\text{shots}}^{5\sigma, \pi/2}$, which are also shown in Tab. (III). Comparing with Tab. (II) we see that over an order of magnitude *fewer* shots would be required to determine the experimental values of the fundamental low energy constants $c_{4,1}$ and $c_{4,2}$ to 5σ statistical significance. This is also seen in Fig. (14), which shows how the number of shots required for 5σ significance in the polarisation insensitive measurement varies with the background using the estimated number of signal photons from Tab. (III).

	$f^\#$	$N_{\gamma,*}(\pi/4)$	$N_{\gamma,*}(\pi/2)$	N_γ^{bg}	$N_{\text{shots}}^{3\sigma}$	$N_{\text{shots}}^{5\sigma}$
EU.XFEL	1	2.4×10^{-3}	3.6×10^{-3}	6.3×10^{-7}	4.2×10^2	1.2×10^3
	2	7.9×10^{-4}	1.2×10^{-3}	6.3×10^{-7}	1.5×10^3	4.2×10^3
SACLA	1	3.3×10^{-2}	5.0×10^{-2}	2.5×10^{-7}	2.1×10^1	5.8×10^1
	2	8.4×10^{-3}	1.3×10^{-2}	2.5×10^{-7}	9.3×10^1	2.6×10^2

TABLE III. Estimated number of signal photons in a polarisation insensitive measurement, $N_{\gamma,*}(\Delta\psi)$, for different polarisation differences $\Delta\psi$, alongside associated background, N_γ^{bg} . Estimates account for the use of two standard beryllium lenses with 50% transmission to focus the probe and scattered beams. Also shown is estimated number of shots $N_{\text{shots}}^{n\sigma} = N_{\text{shots}}^{n\sigma, \frac{\pi}{4}} + N_{\text{shots}}^{n\sigma, \frac{\pi}{2}}$ required for 3σ and 5σ statistical significance, calculated assuming an optimal collision of the beams.

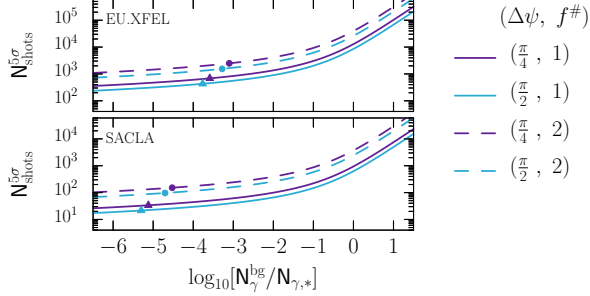


FIG. 14. Estimated number of shots required to achieve 5σ significance as a function of the ratio $N_\gamma^{\text{bg}}/N_{\gamma,*}$. X-ray and optical pulse parameters as in Fig. (12) with $\Theta = 45^\circ$. Estimations of number of signal photons held fixed and given in Tab. (III). *Purple solid*: $f^\# = 1$ parallel. *Blue solid*: $f^\# = 1$ perpendicular. *Purple dashed*: $f^\# = 2$ parallel. *Blue dashed*: $f^\# = 2$ perpendicular. The data points correspond to the background estimations in Tab. (III).

When considering the birefringent signal, it was possible to demonstrate through Fig. (7) that the ratio of the number of perpendicular to parallel polarised signal photons follow simple analytical relationships which depend only on the fundamental low-energy constants of the LO process and the polarisation difference, Eq. (32). We can demonstrate an analogous relationship in the polarisation insensitive measurement by instead considering the ratio of the total number of signal photons due to different polarisation differences, $\Delta\psi \neq \Delta\psi'$, see Eq. (33). This is shown in Fig. (15) for a fixed collision angle of $\Theta = 30^\circ$ for $f^\# = 1$ optical focussing. We take as a reference value the number of signal photons at $\Delta\psi' = \pi/2$, $N'_{\gamma,*} \equiv N_{\gamma,*}(\pi/2)$, and use this to normalise the number of photons as a function of $\Delta\psi$, $N_{\gamma,*}(\Delta\psi)$. This normalisation ensures that all of the spacetime dependent factors cancel, and we see that the simple analytical ratio Eq. (33) agrees with the numerically evaluated data for both EU.XFEL (purple circles) and SACLA (blue triangles) SASE parameters.

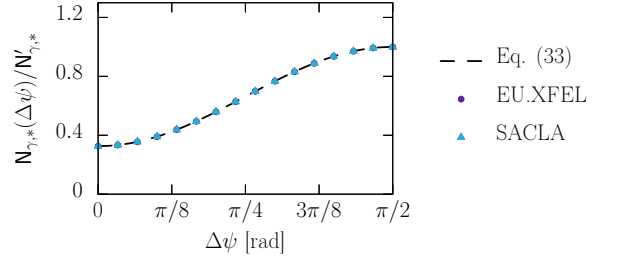


FIG. 15. Ratio of total number of scattered photons at different relative polarisations, $N_{\gamma,*}(\Delta\psi)/N_{\gamma,*}(\Delta\psi')$. The reference relative polarisation is chosen as $\Delta\psi' = \pi/2$. X-ray and optical pulse parameters as in Fig. (12). *Black dashed*: Ratio Eq. (33) for $\Delta\psi' = \pi/2$. *Purple circle*: EU.XFEL SASE parameters. *Blue triangle*: SACLA SASE parameters.

2. Next generation technology: 6-photon scattering

We now consider a measurement of unpolarised photon-photon scattering with an upgraded optical laser Tab. (I) as in Sec. VB2 (with $w_x = 2 \mu\text{m}$, $f^\# = 2$, $\theta_* = 450 \mu\text{rad}$). The polarisation ψ is chosen to optimise the number of scattered photons: $\psi_x = \psi_0 = \psi$. Fig. (16) shows the dependence of the total number of signal photons with $\theta_\gamma > \theta_*$, $N_{\gamma,*}$, on the collision angle Θ at fixed $\psi = 0$. The use of SASE parameters has increased the number of photons with $\theta_x > \theta_*$ to a peak of $N_{\gamma,*} \approx 1.2 \times 10^{-4}$ at $\Theta = 63^\circ$. While still small, this is a large improvement over the polarisation sensitive measurement outlined in Sec. VB2.

Just as in the LO case, we need two independent measurements to be able to experimentally determine the values of the 6-photon low-energy constants, theoretically predicted as in Eq. (35). The two observables are chosen as the total number of signal photons at two different values of the polarisation parameter ψ . The dependence of the total number of signal photons on ψ is shown in Fig. (17). We have chosen the collision angle $\Theta = 63^\circ$ around which the number of signal photons has a maximum in Fig. (16). In this case we find, including the effect of

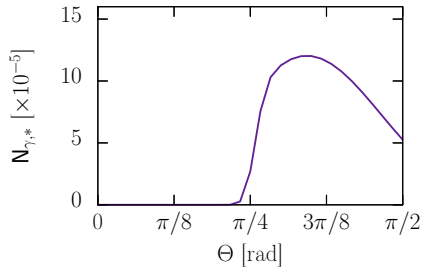


FIG. 16. Total number of signal photons with $\theta_\gamma > \theta_*$ vs collision angle Θ from the collision of EU.XFEL SASE $\omega_x = 10$ keV photons with future generation laser. All other pulse parameters are as in Fig. (9).

x-ray focussing optics,

$$\frac{N_{\gamma,*}(0) \quad N_{\gamma,*}(\pi/2)}{3.0 \times 10^{-5} \quad 8.8 \times 10^{-6}} \Big| \frac{N_\gamma^{\text{bg}}}{6.3 \times 10^{-7}} \quad (47)$$

with the estimated backgrounds being the same as in the preceding section. We estimate that $N_{\text{shots}}^{5\sigma} \gtrsim 1.1 \times 10^6$ shots would be required to determine the 6-photon low-energy constants to 5σ significance.

VI. SUMMARY

Real photon-photon scattering has yet to be experimentally verified. Measuring either the unpolarised or the polarised case (vacuum birefringence) would allow confirmation of an outstanding prediction from quantum electrodynamics (QED) for the magnitude of fundamental low-energy constants that govern the effective non-linear coupling of photons with one other. Measurement of the effective photon-photon coupling could be used to place bounds on new physics beyond the Standard Model [55, 57, 91–96] and act as a gateway to harnessing the nonlinear vacuum for more exotic applications such as vacuum high harmonic generation and self-focussing.

We have shown that there are several advantages in using a planar three-beam set-up to measure photon-photon scattering. The kinematics allow for photons to be scattered into Bragg side-peaks in the detector plane, thereby providing spatial separation of the signal from the large photon background and significantly increasing the signal-to-noise ratio compared to the more conventional two-beam set-up. In the planar three-beam set-up: i) the fundamental low-energy QED constants can be determined by measuring numbers of scattered photons, without the need for polarimetry; ii) since the bandwidth of the x-ray beam does not have to be especially low for polarimetry purposes, an XFEL seeding mode such as SASE can be used that increases the photon-photon scattering signal; iii) higher orders of photon-photon scattering lead to further Bragg side-peaks that

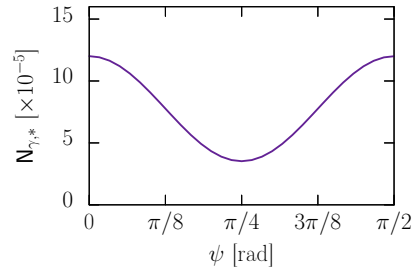


FIG. 17. Number of signal photons vs polarisation ψ from the collision of EU.XFEL SASE $\omega_x = 10$ keV photons with a next generation multi-kJ laser system at a collision angle of $\Theta = 63^\circ$. All other x-ray and optical pulse parameters as in Fig. (9).

correlate transverse detector position with expansion order of the effective photon-photon interaction. This in principle allows the determination of fundamental low-energy QED constants for higher dimensional terms that lead to e.g. six-photon scattering. These considerations further emphasise the point that configurations of lasers that are beyond plane waves can support processes that are otherwise kinematically suppressed in the plane wave case.

Specifically, we calculated the number of scattered photons if an XFEL provides the probe field and two high power optical beams provide the pump field. Two different parameter sets were considered. Firstly, currently available technology was shown to be sufficient to measure 4-photon scattering; parameters were chosen from those available at the EU.XFEL, which will be used in the proposed BIREF@HIBEF experiment [70, 82], and those available at SACLA. We found that the number of required shots to obtain a 5σ significance value using the three-beam scenario, c.f. Tab. (II) and Tab. (III), could be competitive with, and/or complementary to, other approaches such as the dark-field method [56, 82]. Secondly, we considered future technology to measure 6-photon scattering with the EU.XFEL and an optical laser capable of reaching intensities of $\sim 10^{24} - 10^{25} \text{ Wcm}^{-2}$, such as may be achievable at the Station of Extreme Light [40]. Alternatively, future parameters to increase the 6-photon signal could involve increasing the brilliance of the XFEL beam or the frequency of collisions with the optical beams.

ACKNOWLEDGMENTS

AJM is supported by the project ‘‘Advanced Research Using High Intensity Laser Produced Photons and Particles’’ (ADONIS) CZ.02.1.01/0.0/0.0/16_019/0000789 from European Regional Development Fund (ERDF). The authors thank Sergei V. Bulanov for useful discus-

sions.

Appendix A: Beam field profiles

In this appendix we give more details about the field profiles of the three input beams to our configuration. The XFEL beam and the two optical beams are all described by Gaussian focussed pulses in the paraxial approximation. The normalised electric field profiles, $E_i(x)$, are,

$$E_i(x) = \frac{\mathcal{E}_i}{\sqrt{1 + \zeta_i^2}} e^{-\frac{(x_i^\perp)^2}{w_i^2(1 + \zeta_i^2)} - \frac{(k_i \cdot x)^2}{\Phi_i^2}} \times \cos \left[k_i \cdot x + \tan^{-1} \zeta_i - \frac{(x_i^\perp)^2 \zeta_i}{w_i^2(1 + \zeta_i^2)} \right], \quad (\text{A1})$$

where $\zeta_i = \mathbf{k}_i \cdot x / \omega_i z_{R,i}$ is the curvature parameter defined in terms of the Rayleigh length $z_{R,i} = \omega w_i^2 / 2$, with w_i defined as the distance from the focus at which the peak intensity is reduced by a factor $1/e^2$, and \mathbf{k}_i , the 3-wavevector of k_i^μ . The phase duration of the pulses is $\Phi_i = \omega_i \tau_i$, with τ_i the temporal duration at which the pulse intensity falls to $1/e^2$ of the peak. The field strengths \mathcal{E}_i can be expressed in terms of the total energy of the pulse as [97],

$$\mathcal{E}_x^2 = 8 \sqrt{\frac{2}{\pi}} \frac{N_x \omega_x}{E_{cr}^2 \pi w_x^2 \tau_x}, \quad \mathcal{E}_1^2 = \mathcal{E}_2^2 = \mathcal{E}_0^2 = 8 \sqrt{\frac{2}{\pi}} \frac{W}{E_{cr}^2 \pi w_0^2 \tau_0}, \quad (\text{A2})$$

where for simplicity we consider both the optical lasers to have the same field strength and, waist, and duration, N_x is the number of photons in the x-ray pulse and W is the energy of the optical pulses. The coordinates x_i^\perp denote the directions transverse to the beam propagation direction. With the wavevectors outlined in Sec. III, the transverse coordinates are, for k_x^μ ,

$$(x_x^\perp)^2 = x^2 + y^2, \quad (\text{A3})$$

for $k_1^\mu(\Theta)$,

$$(x_1^\perp)^2 = (x \cos \theta + z \sin \theta)^2 + y^2, \quad (\text{A4})$$

and for $k_2^\mu(\Theta)$,

$$(x_2^\perp)^2 = (x \cos \theta - z \sin \theta)^2 + y^2. \quad (\text{A5})$$

The signal photons, k_γ^μ , are taken to be plane wave states,

$$F_\gamma^{\mu\nu}(x) = \frac{1}{\omega_\gamma} (k_\gamma^\mu \varepsilon_\gamma^\nu - k_\gamma^\nu \varepsilon_\gamma^\mu) E_\gamma(x), \quad (\text{A6})$$

with

$$E_\gamma(x) = \frac{1}{E_{cr}} \sqrt{\frac{\omega_\gamma}{2V}} e^{ik_\gamma \cdot x}, \quad (\text{A7})$$

and V a volumetric normalisation.

Numerical results presented in Sec. V have primarily been obtained using the ‘‘infinite Rayleigh length approximation’’ (IRLA), where $\zeta_i \rightarrow 0$ in Eq. (A1) [15, 20, 53, 76, 98]. In the planar three-beam collision considered in this paper, the functional dependence of the beam profiles Eq. (A1) mean that the temporal and out-of-plane coordinate integrals in Eq. (5) and (9) can be performed analytically, as they are Gaussian. However, with the IRLA the form of the beam profiles simplify considerably,

$$\lim_{\zeta_i \rightarrow 0} E_i(x) = \mathcal{E}_i e^{-\frac{(x_i^\perp)^2}{w_i^2} - \frac{(k_i \cdot x)^2}{\Phi_i^2}} \cos[k_i \cdot x], \quad (\text{A8})$$

allowing *all* of the coordinate integrals in Eq. (5) and (9) to be performed analytically. In Fig. (18) we show the relative error

$$E = 1 - \frac{N_{\gamma,*}^{\text{full}}}{N_{\gamma,*}^{\text{IRLA}}},$$

between the number of signal photons calculated with the full Gaussian pulses in the paraxial approximation Eq. (A1), N_γ^{full} , and the IRLA Eq. (A8), N_γ^{IRLA} . The purple lines correspond to the currently available parameters EUXFEL parameters used in Fig. (12), with the solid line for all signal photons N_γ and the dashed line for only photons within the acceptance region of the detector with $\theta_\gamma > \theta_* = 200 \mu\text{rad}$. The blue dashed line is for the number of photons on the detector acceptance region $\theta_\gamma > \theta_* = 450 \mu\text{rad}$ using the future parameters from Fig. (16). We find that for the case of including all signal photons the IRLA agrees very well with the results using the full Gaussian pulse in the paraxial approximation, with $E \lesssim 5\%$ across the full range of the collision angle Θ . When the detector cut is included, for both currently available and future parameters, we find that for collision angles $\Theta \lesssim 40^\circ$ the error becomes quite large, but as the collision angle increases this rapidly falls to the level of $E \lesssim 1\%$. This can be understood by considering what happens when the collision angle Θ is increased from $\Theta = 0$. Initially, the Bragg side-peaks are emitted head-on and are excluded by the detector cut. As Θ is increased, the centre of the Bragg side-peaks move to larger θ_γ and eventually to values large enough for their outer edges to fall on the detector. To describe the side-peak edges accurately, wavefront curvature and the Gouy phase must be included, so for these values of Θ , where the signal is low, the IRLA makes a significant error. By experimenting turning on and off various terms in the paraxial beam Eq. (A1), it can be confirmed that the main error is made when both the wavefront curvature and the Gouy terms in the phase are neglected in this cut side-peak region. Once the collision angle Θ is increased further so that the Bragg side-peak signal is fully on the detector, the error in the IRLA falls to a very low value. Most importantly, at the collision angle which maximises $N_{\gamma,*}$ for the currently available parameters, $\Theta = 45^\circ$ (vertical dashed lines), and for the future

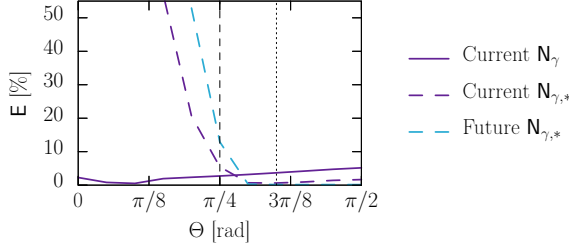


FIG. 18. Relative error $E = 1 - N_{\gamma,*}^{\text{full}}/N_{\gamma,*}^{\text{IRLA}}$ between the number of signal photons calculated with the full Gaussian pulses in the paraxial approximation, $N_{\gamma,*}^{\text{full}}$, and with the IRLA $N_{\gamma,*}^{\text{IRLA}}$. Also shown are the collision angles at which the number of signal photons is maximised for the currently available parameters (vertical dashed) and future parameters (vertical dotted).

parameters, $\Theta = 63^\circ$ (vertical dotted lines), the relative error is on the level of $E \approx 5\%$ and $E \approx 0.2\%$, respectively.

-
- [1] F. Sauter, Z. Phys. **69**, 742 (1931).
[2] O. Halpern, Phys. Rev. **44**, 855.2 (1933).
[3] W. Heisenberg, Z. Phys. **90**, 209 (1934), english translation: *Remarks on the Dirac theory of the positron*, in A. I. Miller, *Early Quantum Electrodynamics*, pp. 169-187, Cambridge UP, 1995. [Erratum: Z.Phys. 92, 692-692 (1934)].
[4] W. Heisenberg and H. Euler, Z. Phys. **98**, 714 (1936), arXiv:physics/0605038.
[5] J. S. Schwinger, Phys. Rev. **82**, 664 (1951).
[6] J. S. Toll, (1952), PhD thesis, Princeton.
[7] M. Delbrück, Z. Phys. **84**, 144 (1933).
[8] M. Schumacher, I. Borchert, F. Smend, and P. Rullhusen, Phys. Lett. B **59**, 134 (1975).
[9] M. Aaboud *et al.* (ATLAS), Nature Phys. **13**, 852 (2017), arXiv:1702.01625 [hep-ex].
[10] G. Aad *et al.* (ATLAS), Phys. Rev. Lett. **123**, 052001 (2019), arXiv:1904.03536 [hep-ex].
[11] A. M. Sirunyan *et al.* (CMS), Phys. Lett. B **797**, 134826 (2019), arXiv:1810.04602 [hep-ex].
[12] J. D. Brandenburg, J. Seger, Z. Xu, and W. Zha, Rept. Prog. Phys. **86**, 083901 (2023), arXiv:2208.14943 [hep-ph].
[13] J. Adam *et al.* (STAR), Phys. Rev. Lett. **127**, 052302 (2021), arXiv:1910.12400 [nucl-ex].
[14] A. Di Piazza, K. Z. Hatsagortsyan, and C. H. Keitel, Phys. Rev. Lett. **97**, 083603 (2006), arXiv:hep-ph/0602039.
[15] B. King, A. Di Piazza, and C. H. Keitel, Nature Photon. **4**, 92 (2010), arXiv:1301.7038 [physics.optics].
[16] B. King, A. Di Piazza, and C. H. Keitel, Phys. Rev. A **82**, 032114 (2010), arXiv:1301.7008 [physics.optics].
[17] G. Y. Kryuchkyan and K. Z. Hatsagortsyan, Phys. Rev. Lett. **107**, 053604 (2011).
[18] D. Tommasini and H. Michinel, Phys. Rev. A **82**, 011803 (2010), arXiv:1003.5932 [hep-ph].
[19] Y. Monden and R. Kodama, Phys. Rev. Lett. **107**, 073602 (2011).
[20] B. King and C. H. Keitel, New J. Phys. **14**, 103002 (2012), arXiv:1202.3339 [hep-ph].
[21] B. Jin, B. Shen, and D. Xu, Phys. Rev. A **106**, 013502 (2022).
[22] H. Gies, F. Karbstein, and N. Seegert, New J. Phys. **15**, 083002 (2013), arXiv:1305.2320 [hep-ph].
[23] E. Lundstrom, G. Brodin, J. Lundin, M. Marklund, R. Bingham, J. Collier, J. T. Mendonca, and P. Norreys, Phys. Rev. Lett. **96**, 083602 (2006), arXiv:hep-ph/0510076.
[24] H. Gies, F. Karbstein, and R. Shaisultanov, Phys. Rev. D **90**, 033007 (2014), arXiv:1406.2972 [hep-ph].
[25] R. Aboushelbaya *et al.*, Phys. Rev. Lett. **123**, 113604 (2019), arXiv:1902.05928 [physics.optics].
[26] M. Formanek, J. P. Palastro, D. Ramsey, S. Weber, and A. Di Piazza, Phys. Rev. D **109**, 056009 (2024), arXiv:2307.11734 [hep-ph].
[27] B. Jin and B. Shen, Phys. Rev. A **107**, 062213 (2023).
[28] A. V. Berezin and A. M. Fedotov, (2024), arXiv:2405.00151 [hep-ph].
[29] M. Valialshchikov, F. Karbstein, D. Seipt, and M. Zepf, (2024), arXiv:2405.03317 [hep-ph].
[30] N. N. Rozanov, Zhurnal Eksperimentalnoi i Teoreticheskoi Fiziki **103**, 1996 (1993).
[31] A. Di Piazza, K. Z. Hatsagortsyan, and C. H. Keitel, Phys. Rev. D **72**, 085005 (2005).
[32] A. Fedotov and N. Narozhny, Physics Letters A **362**, 1 (2007).
[33] J. S. Heyl and L. Hernquist, Phys. Rev. D **59**, 045005 (1999), arXiv:hep-th/9811091.
[34] P. Böhl, B. King, and H. Ruhl, Phys. Rev. A **92**, 032115 (2015), arXiv:1503.05192 [physics.plasm-ph].
[35] M. Marklund and P. K. Shukla, Rev. Mod. Phys. **78**, 591 (2006).
[36] A. Di Piazza, C. Müller, K. Z. Hatsagortsyan, and C. H. Keitel, Rev. Mod. Phys. **84**, 1177 (2012).
[37] B. King and T. Heinzl, High Power Laser Sci. Eng. **4** (2016), 10.1017/hpl.2016.1, arXiv:1510.08456 [hep-ph].
[38] A. Fedotov, A. Ilderton, F. Karbstein, B. King, D. Seipt, H. Taya, and G. Torgrimsson, (2022), arXiv:2203.00019 [hep-ph].
[39] S. Weber *et al.*, Matter Radiat. Extremes **2**, 149 (2017).
[40] B. Shen, Z. Bu, J. Xu, T. Xu, L. Ji, R. Li, and Z. Xu, Plasma Phys. Control. Fusion **60**, 044002 (2018).

- [41] C. N. Danson *et al.*, High Power Laser Science and Engineering **7**, e54 (2019).
- [42] D. Xu, B. Shen, J. Xu, and Z. Liang, Nuclear Instruments and Methods in Physics Research Section A: Accelerators, Spectrometers, Detectors and Associated Equipment **982**, 164553 (2020).
- [43] A. D. Piazza, L. Willingale, and J. D. Zuegel, “Multi-petawatt physics prioritization (mp3) workshop report,” (2022), arXiv:2211.13187 [hep-ph].
- [44] V. Dinu, T. Heinzl, A. Ilderton, M. Marklund, and G. Torgrimsson, Phys. Rev. D **89**, 125003 (2014), arXiv:1312.6419 [hep-ph].
- [45] V. Dinu, T. Heinzl, A. Ilderton, M. Marklund, and G. Torgrimsson, Phys. Rev. D **90**, 045025 (2014), arXiv:1405.7291 [hep-ph].
- [46] S. Bragin, S. Meuren, C. H. Keitel, and A. Di Piazza, Phys. Rev. Lett. **119**, 250403 (2017), arXiv:1704.05234 [hep-ph].
- [47] S. Meuren, K. Z. Hatsagortsyan, C. H. Keitel, and A. Di Piazza, Phys. Rev. Lett. **114**, 143201 (2015), arXiv:1407.0188 [hep-ph].
- [48] B. King and N. Elkina, Phys. Rev. A **94**, 062102 (2016), arXiv:1603.06946 [hep-ph].
- [49] A. J. Macleod, J. P. Edwards, T. Heinzl, B. King, and S. V. Bulanov, New J. Phys. **25**, 093002 (2023), arXiv:2304.02114 [hep-ph].
- [50] F. Moulin and D. Bernard, Optics Communications **164**, 137 (1999).
- [51] J. Lundin, M. Marklund, E. Lundstrom, G. Brodin, J. Collier, R. Bingham, J. T. Mendonca, and P. Norreys, Phys. Rev. A **74**, 043821 (2006), arXiv:hep-ph/0606136.
- [52] H. Gies, F. Karbstein, C. Kohlfürst, and N. Seegert, Phys. Rev. D **97**, 076002 (2018), arXiv:1712.06450 [hep-ph].
- [53] B. King, H. Hu, and B. Shen, Phys. Rev. A **98**, 023817 (2018), arXiv:1805.03688 [hep-ph].
- [54] N. Ahmadinia, T. E. Cowan, J. Grenzer, S. Franchino-Viñas, A. L. Garcia, M. Smid, T. Toncian, M. A. Trejo, and R. Schützhold, (2022), arXiv:2208.14215 [physics.optics].
- [55] M. Fouché, R. Battesti, and C. Rizzo, Phys. Rev. D **93**, 093020 (2016), [Erratum: Phys.Rev.D 95, 099902 (2017)], arXiv:1605.04102 [physics.optics].
- [56] F. Karbstein, D. Ullmann, E. A. Mosman, and M. Zepf, Phys. Rev. Lett. **129**, 061802 (2022), arXiv:2207.09866 [hep-ph].
- [57] A. Ejlli, F. Della Valle, U. Gastaldi, G. Messineo, R. Pengo, G. Ruoso, and G. Zavattini, Phys. Rept. **871**, 1 (2020), arXiv:2005.12913 [physics.optics].
- [58] K. S. Schulze, B. Grabiger, R. Loetzsch, B. Marx-Glowna, A. T. Schmitt, A. L. Garcia, W. Hippler, L. Huang, F. Karbstein, Z. Konôpková, H.-P. Schlenvoigt, J.-P. Schwinkendorf, C. Strohm, T. Toncian, I. Uschmann, H.-C. Wille, U. Zastra, R. Röhlberger, T. Stöhlker, T. E. Cowan, and G. G. Paulus, Phys. Rev. Res. **4**, 013220 (2022).
- [59] A. Kondratenko and E. Saldin, Part. Accel. **10**, 207 (1980).
- [60] R. Bonifacio, C. Pellegrini, and L. Narducci, Optics Communications **50**, 373 (1984).
- [61] V. B. Berestetskii, E. M. Lifshitz, and L. P. Pitaevskii, *QUANTUM ELECTRODYNAMICS*, Course of Theoretical Physics, Vol. 4 (Pergamon Press, Oxford, 1982).
- [62] B. De Tollis, Nuovo Cim. **35**, 1182 (1965).
- [63] Z. Huang and K.-J. Kim, Phys. Rev. ST Accel. Beams **10**, 034801 (2007).
- [64] B. W. McNeil and N. R. Thompson, Nature photonics **4**, 814 (2010).
- [65] C. Pellegrini, A. Marinelli, and S. Reiche, Rev. Mod. Phys. **88**, 015006 (2016).
- [66] C. Feng and H.-X. Deng, Nuclear Science and Techniques **29**, 160 (2018).
- [67] N. Huang, H. Deng, B. Liu, D. Wang, and Z. Zhao, The Innovation **2** (2021).
- [68] T. Heinzl, B. Liesfeld, K.-U. Amthor, H. Schwöerer, R. Sauerbrey, and A. Wipf, Opt. Commun. **267**, 318 (2006), arXiv:hep-ph/0601076.
- [69] F. Karbstein, H. Gies, M. Reuter, and M. Zepf, Phys. Rev. D **92**, 071301 (2015), arXiv:1507.01084 [hep-ph].
- [70] H.-P. Schlenvoigt, T. Heinzl, U. Schramm, T. E. Cowan, and R. Sauerbrey, Phys. Scripta **91**, 023010 (2016).
- [71] T. Inada, T. Yamazaki, T. Yamaji, Y. Seino, X. Fan, S. Kamioka, T. Namba, and S. Asai, Science **7**, 671 (2017), arXiv:1707.00253 [hep-ex].
- [72] S. Shakeri, S. Z. Kalantari, and S.-S. Xue, Phys. Rev. A **95**, 012108 (2017), arXiv:1703.10965 [hep-ph].
- [73] S. Huang, B. Jin, and B. Shen, Phys. Rev. D **100**, 013004 (2019).
- [74] Y. Seino, T. Inada, T. Yamazaki, T. Namba, and S. Asai, PTEP **2020**, 073C02 (2020), arXiv:1912.01390 [hep-ph].
- [75] A. T. Schmitt *et al.*, Optica **8**, 56 (2021), arXiv:2003.00849 [physics.ins-det].
- [76] F. Karbstein, C. Sundqvist, K. S. Schulze, I. Uschmann, H. Gies, and G. G. Paulus, New J. Phys. **23**, 095001 (2021), arXiv:2105.13869 [hep-ph].
- [77] Q. Yu, D. Xu, B. Shen, T. E. Cowan, and H.-P. Schlenvoigt, High Power Laser Science and Engineering **11**, e71 (2023).
- [78] J. Wang, G. Y. Chen, B. F. Lei, S. Jin, L. Y. Yang, L. F. Gan, C. T. Zhou, S. P. Zhu, X. T. He, and B. Qiao, New J. Phys. **26**, 023008 (2024).
- [79] D. Galtsov and V. Skobelev, Physics Letters B **36**, 238 (1971).
- [80] V. Ritus, J. Exp. Theor. Phys. **42**, 774 (1975).
- [81] E. A. Mosman and F. Karbstein, Phys. Rev. D **104**, 013006 (2021), arXiv:2104.05103 [hep-ph].
- [82] N. Ahmadinia *et al.*, (2024), arXiv:2405.18063 [physics.ins-det].
- [83] T. Yabuuchi, A. Kon, Y. Inubushi, T. Togahi, K. Sueda, T. Itoga, K. Nakajima, H. Habara, R. Kodama, H. Tomizawa, *et al.*, Journal of synchrotron radiation **26**, 585 (2019).
- [84] I. Inoue, T. Osaka, T. Hara, T. Tanaka, T. Inagaki, T. Fukui, S. Goto, Y. Inubushi, H. Kimura, R. Kinjo, *et al.*, Nature photonics **13**, 319 (2019).
- [85] J. Feldhaus, E. Saldin, J. Schneider, E. Schneidmiller, and M. Yurkov, Optics Communications **140**, 341 (1997).
- [86] V. K. Gianluca Geloni and E. Saldin, Journal of Modern Optics **58**, 1391 (2011), <https://doi.org/10.1080/09500340.2011.586473>.
- [87] A. Laso Garcia, H. Höppner, A. Pelka, C. Bähz, E. Brambrink, S. Di Dio Cafiso, J. Dreyer, S. Göde, M. Hassan, T. Kluge, and *et al.*, High Power Laser Science and Engineering **9**, e59 (2021).
- [88] G. Cowan, K. Cranmer, E. Gross, and O. Vitells, Eur. Phys. J. C **71**, 1554 (2011), [Erratum: Eur.Phys.J.C 73, 2501 (2013)], arXiv:1007.1727 [physics.data-an].
- [89] N. Ahmadinia, T. E. Cowan, M. Ding, M. A. L. Lopez,

- R. Sauerbrey, R. Shaisultanov, and R. Schützhold, (2022), arXiv:2212.03350 [hep-ph].
- [90] G. Geloni, V. Kocharyan, and E. Saldin, *Optics Communications* **356**, 435 (2015).
- [91] M. Ahlers, H. Gies, J. Jaeckel, J. Redondo, and A. Ringwald, *Phys. Rev. D* **77**, 095001 (2008), arXiv:0711.4991 [hep-ph].
- [92] H. Gies, *Eur. Phys. J. D* **55**, 311 (2009), arXiv:0812.0668 [hep-ph].
- [93] S. Villalba-Chávez, T. Podszus, and C. Müller, *Phys. Lett. B* **769**, 233 (2017), arXiv:1612.07952 [hep-ph].
- [94] S. Villalba-Chávez, S. Meuren, and C. Müller, *Phys. Lett. B* **763**, 445 (2016), arXiv:1608.08879 [hep-ph].
- [95] K. A. Beyer, G. Marocco, R. Bingham, and G. Gregori, *Phys. Rev. D* **101**, 095018 (2020), arXiv:2001.03392 [hep-ph].
- [96] S. Evans and R. Schützhold, *Phys. Rev. D* **109**, L091901 (2024), arXiv:2307.08345 [hep-ph].
- [97] F. Karbstein and E. A. Mosman, *Phys. Rev. D* **96**, 116004 (2017), arXiv:1711.06151 [hep-ph].
- [98] H. Gies, F. Karbstein, and C. Kohlfürst, *Phys. Rev. D* **97**, 036022 (2018), arXiv:1712.03232 [hep-ph].